Journal of Sea Research 125 (2017) 1–17

Contents lists available at ScienceDirect

Journal of Sea Research

journal homepage: www.elsevier.com/locate/seares

Modelling Kara Sea phytoplankton primary production: Development and skill assessment of regional algorithms

Andrey B. Demidov[a,*], Oleg V. Kopelevich[a], Sergey A. Mosharov[a,b], Sergey V. Sheberstov[a], Svetlana V. Vazyulya[a]

[a] P.P. Shirshov Institute of Oceanology, Russian Academy of Sciences, 117997 Moscow, Nachimovsky av. 36, Russia
[b] Bauman Moscow State Technical University, 105005 Moscow, 2 Baumanskaya st. 5, Russia

ARTICLE INFO

Keywords:
Primary production
Chlorophyll *a*
Kara Sea
Modelling primary production
Chlorophyll specific carbon fixation rate
Efficiency of photosynthesis

ABSTRACT

Empirical region-specific (RSM), depth-integrated (DIM) and depth-resolved (DRM) primary production models are developed based on data from the Kara Sea during the autumn (September–October 1993, 2007, 2011). The model is validated by using field and satellite (MODIS-Aqua) observations. Our findings suggest that RSM algorithms perform better than non-region-specific algorithms (NRSM) in terms of regression analysis, root-mean-square difference (RMSD) and model efficiency. In general, the RSM and NRSM underestimate or overestimate the *in situ* water column integrated primary production (IPP) by a factor of 2 and 2.8, respectively. Additionally, our results suggest that the model skill of the RSM increases when the chlorophyll specific carbon fixation rate, efficiency of photosynthesis and photosynthetically available radiation (PAR) are used as input variables. The parameterization of chlorophyll (chl *a*) vertical profiles is performed in Kara Sea waters with different trophic statuses. Model validation with field data suggests that the DIM and DRM algorithms perform equally (RMSD of 0.29 and 0.31, respectively). No changes in the performance of the DIM and DRM algorithms are observed (RMSD of 0.30 and 0.31, respectively) when satellite-derived chl *a*, PAR and the diffuse attenuation coefficient (K_d) are applied as input variables.

1. Introduction

Estimating the annual water column integrated primary production (IPP) (symbols and abbreviations are presented in Table 1) and studying its spatiotemporal variability on regional and global scales are among the main tasks of ocean biogeochemistry. Field studies provide *in situ* measurements but cannot quantify basin and global IPP dynamics without significant extrapolation (Berger, 1989; Bidigare et al., 1992; Koblentz-Mishke et al., 1970). This problem can be resolved by using bio-optical high resolution satellite-derived data (*e.g.*, surface chl *a* (Chl_0)), sea surface temperature (T_0) and incident photosynthetically available radiation (PAR) (Carder et al., 2004; McClain et al., 1998, 2004; O'Reilly et al., 1998) as input variables in the IPP models. Therefore, modelling IPP is the key approach in the investigation of primary productivity (*e.g.*, Behrenfeld and Falkowski, 1997b; Carr et al., 2006; Platt and Sathyendranath, 1993).

Numerous IPP algorithm designs and assessments of their predictive capacity on global and regional scales have been developed during the "ocean colour satellite era" (from 1978 to the present) (Campbell et al., 2002; Carr et al., 2006; Friedrichs et al., 2009; Saba et al., 2010, 2011). The results of four Primary Productivity Algorithm Round Robins (PPARR) allowed these authors to come to the following main conclusions: (i) the model's performance was independent of the algorithm's complexity, namely, the number of input variables, depth and wavelength resolution; (ii) all the models over- or underestimated the IPP by approximately a factor of 2; and (iii) the average model skill was significantly lower in shallow regions than in pelagic waters.

The same conclusions could be applied to the Arctic Ocean (AO) (Bélanger et al., 2013; Hill et al., 2013; Hill and Zimmerman, 2010; Matrai et al., 2013; Zhai et al., 2012). Hill and Zimmerman (2010) revealed that AO models over- or underestimated the observed IPP by a factor of 2 and that simple algorithms that were based on chl *a* performed better than more complex algorithms. Recently, descriptions of AO IPP models have been presented in terms of their efficiency (Babin et al., 2015; Y. Lee et al., 2015; Petrenko et al., 2013). These authors concluded that all the AO IPP models currently have significant limitations and should be used with caution.

One important factor causing problems in the development of robust IPP models for the Arctic Ocean is undersampling and a lack of suitable data on primary production and abiotic characteristics.

* Corresponding author.
E-mail address: dempsa@rambler.ru (A.B. Demidov).

http://dx.doi.org/10.1016/j.seares.2017.05.004
Received 12 September 2016; Accepted 11 May 2017
Available online 12 May 2017
1385-1101/

Thus, comparatively few AO region-specific algorithms have been developed with Arctic Ocean datasets (Hill et al., 2013; Hill and Zimmerman, 2010; Matrai et al., 2013; Zhai et al., 2012) and applied to the assessment of AO IPP (Hill et al., 2013).

The accuracy of IPP models that were developed based on the World Ocean dataset decreases at the regional scale, and significant regional differences exist in the performance of algorithms (Campbell et al., 2002; Ishizaka et al., 2007; Z. Lee et al., 2015; Saba et al., 2010; Siegel et al., 2001). Therefore, we can assume that region-specific algorithms perform better than non-regional algorithms. The development of region-specific IPP algorithms for the Kara Sea seems obvious. The Kara Sea is characterized by specific environmental conditions that lead to particular processes of organic matter synthesis because of intense river runoff and a wide shelf zone (Dittmar and Kattner, 2003; Hanzlick and Aagaard, 1980; Holmes et al., 2012; Le Fouest et al., 2013; Stein, 2000). Fresh water discharge into the Kara Sea shelf leads to sharp stratification (Kubryakov et al., 2016; Zatsepin et al., 2010) and high particulate (POM) and coloured dissolved (CDOM) organic matter and terrigenous mineral suspension concentrations (Amon, 2004; Dittmar and Kattner, 2003; Rachold et al., 2004; Vetrov and Romankevich, 2004). Consequently, the Kara Sea waters are characterized by high turbidity, low transparency (average Secchi disk depth (Z_s) of 8 m) and a small photosynthetic layer (Z_{ph}) (22 m on average) (Burenkov et al., 2010; Demidov et al., 2014; Mosharov, 2010; Mosharov et al., 2016; Vedernikov et al., 1994). Therefore, the development of region-specific models could be one method to improve IPP estimation in the Kara Sea's optically complex waters.

Choosing appropriate model coefficients and input variables is very important to increase the algorithm's efficiency. As recently shown, the IPP in the Kara Sea during autumn weakly depends on the chl *a* concentration. On the other hand, the chlorophyll specific carbon fixation rate (P^b_{opt}) and PAR greatly affect the Kara Sea's primary production (Demidov et al., 2014). At the end of the vegetative season, the PAR level should be considered the main factor that defines the primary production in the Kara Sea. Ignoring the chl *a* vertical distribution, specifically, the subsurface chlorophyll maximum (SCM), may be another reason for decreasing of model's efficiency (Ardyna et al., 2013; Arrigo et al., 2011; Hill et al., 2013).

Thus, the main purposes of this study are as follows: (1) the development of a region-specific Kara Sea IPP depth-integrated (DIM) and depth-resolved (DRM) models; (2) the skill assessment of developed models with *in situ* and satellite datasets; (3) a comparison of the predictive skill of region-specific and non-region specific algorithms; (4) the assessment of the effect of photophysiological parameters and PAR on model performance; and (5) the parameterization of vertical chlorophyll profiles in waters with variable productivity and an investigation of the influence of the vertical chl *a* distribution on the model accuracy.

2. Data and methods

2.1. Data sources, sampling and Kara Sea trophic sub-regions

The field data that were used in the model's development were collected during three Kara Sea expeditions: the 49th cruise of the R/V "Dmitry Mendeleev" (from 30 August to 19 September 1993) and the 54th and 59th cruises of the R/V "Akademik Mstislav Keldysh" (from 9 September to 30 September 2007 and from 15 September to 4 October 2011, respectively) (Fig. 1a). Only two stations were established on 30 and 31 August and were included in the autumn database. The chl *a* concentration was measured at 113 stations and the primary production at 85 stations. The PP, chl *a* and PAR data that were used for model validation (Supplementary material S1) were collected at 31 sites during the 125th cruise of the R/V "Professor Shtokman" (from 3 September to 20 September 2013) (Fig. 1b). The PP and chl *a* data and the incident and subsurface PAR (see below) were used to calculate the model coefficients and to obtain the average chl *a* vertical profiles.

The boundaries of the Kara Sea were established in a previous work (Hill et al., 2013). The sampling depths were defined after a preliminary sounding of temperature, conductivity and chlorophyll fluorescence by a CTD probe (Seabird Electronics; SBE-19 and SBE-32). Niskin bottles were deployed at the stations to obtain water samples from discrete depths within the upper 100-m layer. Trace metal cleaning procedures (*e.g.*, Teflon coated covers and springs for the Niskin bottles) were used during all the cruises.

The Chl *a*, PP and PAR data were divided according to the trophic categories as determined by the surface chl *a* concentration (Morel and Berthon, 1989; Uitz et al., 2006) in the following ranges: 0.1–0.5 mg m^{-3} (I); 0.5–1.0 mg m^{-3} (II); 1.0–2.0 mg m^{-3} (III) and > 2 mg m^{-3} (IV). The average trophic level values of the primary productivity and abiotic parameters are presented in Table 2. The relative contributions of waters with different productivity in the Kara Sea regions and water masses (WM) (Demidov et al., 2014; Pivovarov et al., 2003) are presented in Fig. 2. Category I and II waters (Chl_0 = 0.1–1.0 mg m^{-3}) characterize the northern WM. The south-western WM was principally characterized by category I and III waters. Category II and III waters (Chl_0 = 0.5–2.0 mg m^{-3}) primarily characterized the river runoff WM. The high chl *a* concentration in the category IV waters (Chl_0 > 2.0 mg m^{-3}) is an inherent property of the Ob and Enisey estuaries (Fig. 2).

As recommended in previous studies of the vertical chl *a* distribution, stratified and mixed waters should be considered separately. The ratio of photosynthetic to upper mixed layers (Z_{ph}/UML) was chosen as the index of water column stability (Morel and Berthon, 1989; Uitz et al., 2006). Here, we define the photosynthetic layer as the layer up to the compensation depth, where the PP that is measured by the radiocarbon method equals 0. Waters where Z_{ph}/UML > 1 were considered as stratified and Z_{ph}/UML < 1 as mixed. A sharp pycnocline in the upper 10-m layer was observed in the Kara Sea during the autumn (UML = 7–10 m). The photosynthetic layer commonly exceeded the UML and ranged on average from 6 to 47 m in different Kara Sea regions (Demidov et al., 2014). Thus, we considered all the Kara Sea waters as stratified and classified vertical chl *a* profiles according to entirely trophic categories.

2.2. Primary production, chlorophyll and light measurements

The methods for primary production and chl *a* determination are described in detail in previous studies (Mosharov, 2010; Mosharov et al., 2016; Vedernikov et al., 1994) and are summarized in Demidov et al. (2014). Primary production was estimated on board by using a radiocarbon technique (Steemann Nielsen, 1952). The chl *a* concentration was determined by using a spectrophotometric method (Jeffrey and Humphrey, 1975; SCOR–UNESCO, 1966) or fluorometrically (JGOFS, 1994). The PP and chl *a* data that were obtained by these methods were used for model development.

The intensity of the surface irradiance was measured with a pyranometer (Vedernikov et al., 1994) or an LI-190SA (LI-COR) sensor. The daily PAR was obtained from integration in the LI-1400 module for five-minute intervals (mol quanta m^{-2}) and saved in the internal memory. The diffuse attenuation coefficient for downwelling solar radiation in the visible spectrum (K_d) was measured by an alphameter (Vedernikov et al., 1994). In the absence of underwater hydrooptical measurements, K_d was calculated by using empirical Kara Sea region-specific relationships among K_d, the Secchi depth (Z_s) and Chl_0 as shown in the Supplementary material (S2). Vertical profiles of underwater light were retrieved according to Beer's law.

2.3. Satellite ocean colour data, PAR, K_d and chlorophyll region-specific algorithms

Moderate Resolution Imaging Spectroradiometer (MODIS-Aqua)

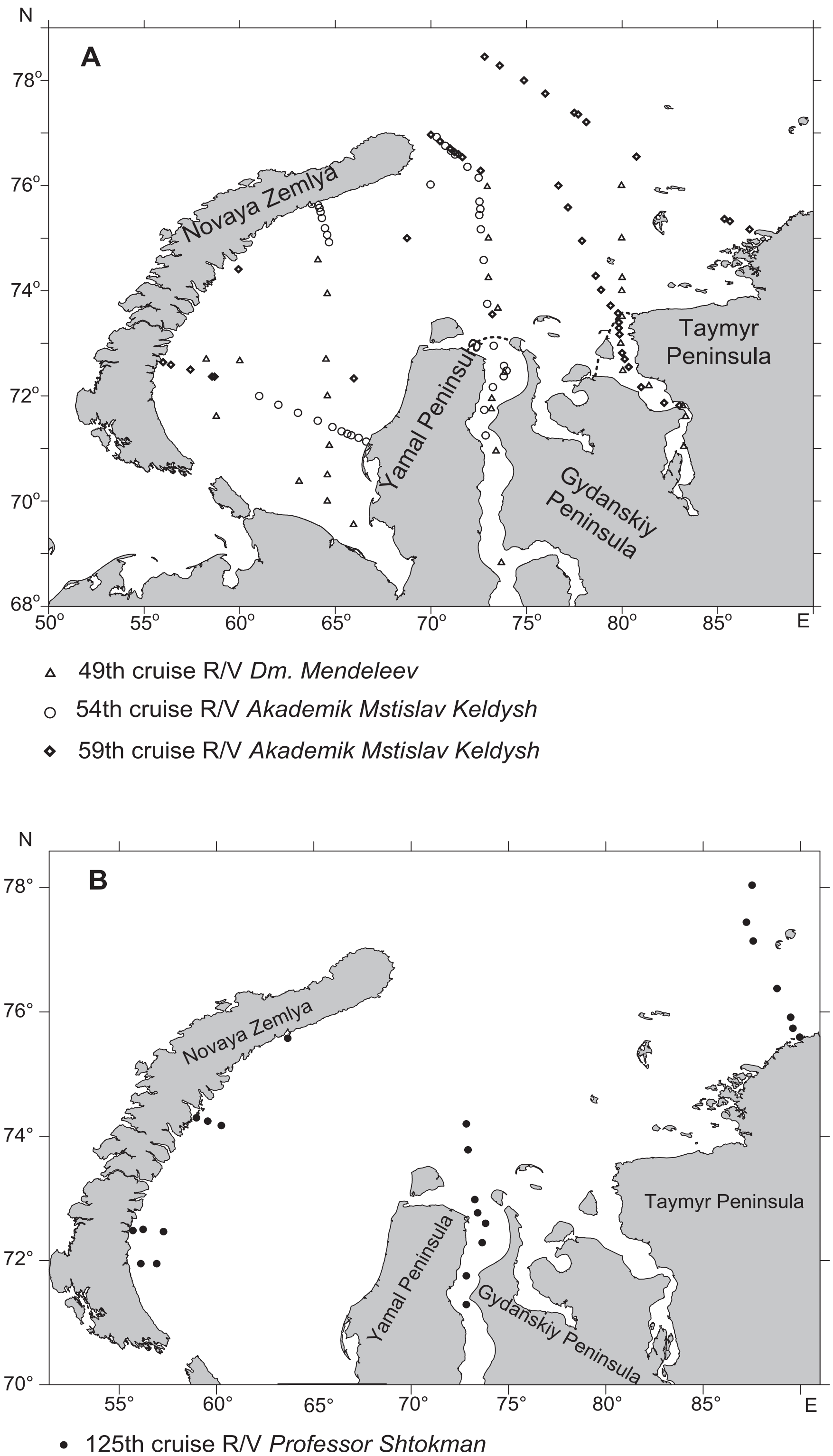

Fig. 1. Maps of the stations that were used for model development (A) and model validation (B).

Level 2 daily water-leaving reflectance (R_{rs}) values at 10 spectral channels (412–869 nm) were obtained from the NASA's Goddard Space Flight Centre (NASA GSFC) (www.oceancolor.gsfc.nasa.gov/). Satellite-derived chl *a*, surface PAR, and diffuse attenuation coefficient (K_d) values were applied as input variables. Keeping in mind specific environmental conditions in the Kara Sea, we used region-specific algorithms to derive Chl and K_d from satellite data; the surface PAR was derived by using the algorithms by Vazyulya et al. (2016).

All the satellite data products were calculated as average values over acceptable pixels around a given point (*in situ* and satellite match-up sites, $N = 26$). A pixel was considered acceptable if it was without flags of cloudiness or land, and $R_{rs} > 0$ for seven considered spectral bands within 488–678 nm; the data were treated by using software that was developed by Sheberstov and Lukyanova (2007).

The chlorophyll concentration was calculated with a novel formula:

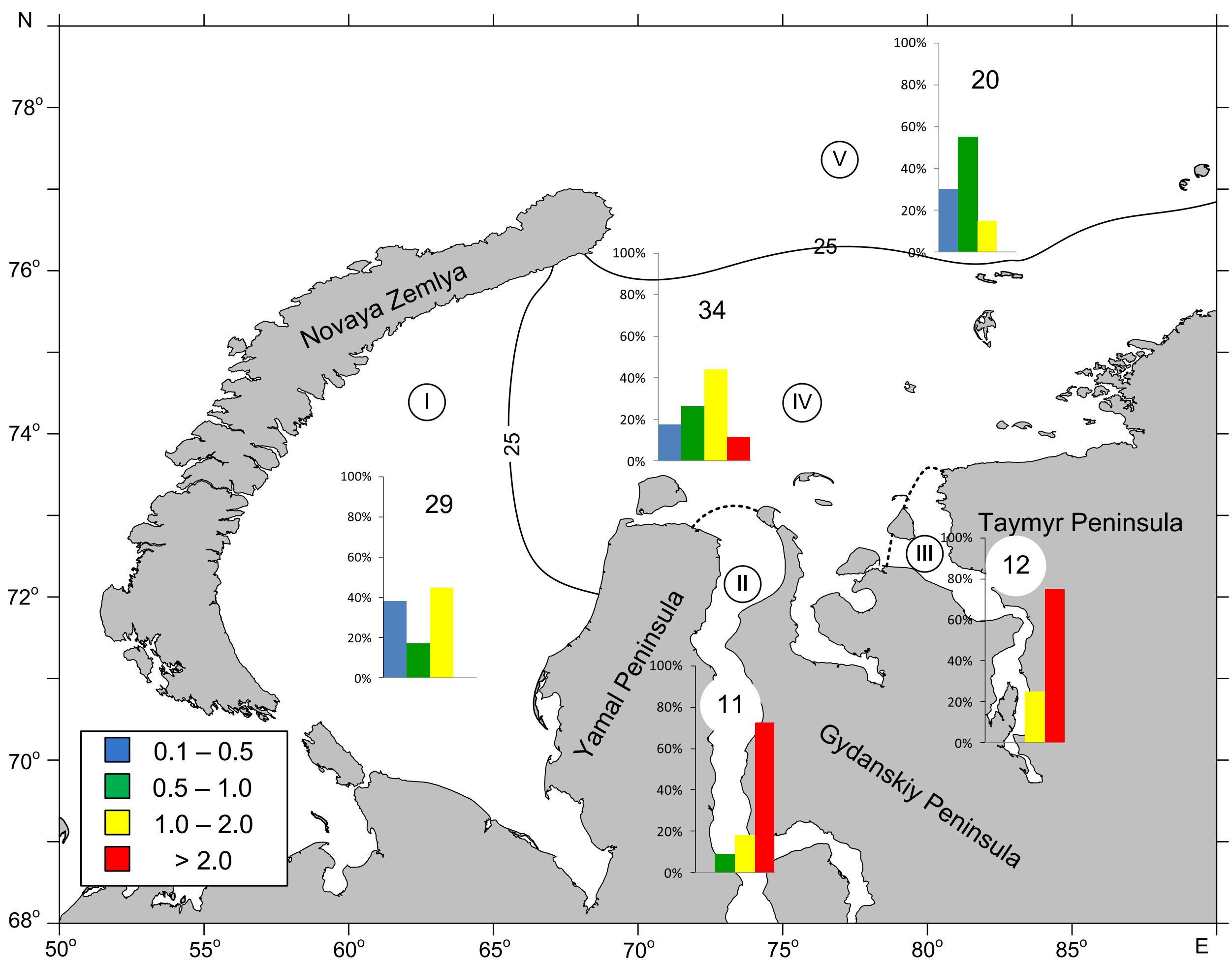

Fig. 2. Contribution (%) of the waters of different productivity (in terms of surface chl *a*, mg m^{-3}) in the Kara Sea water masses (WM) (Demidov et al., 2014; Pivovarov et al., 2003). I – Southwestern WM; II – Ob estuary; III – Enisey estuary; IV – River runoff WM; V – Northern WM (St. Anna's trough). The numerals above the bars are the number of measurements. Surface 25 psu isohaline is shown as a boundary of different WM.

$$\ln(Chl) = -6.64\ \ln\left(R_{rs}(531)/R_{rs}(547)\right) - 0.265\ (R^2 = 0.43; N = 69), \qquad (1)$$

where $R_{rs}(531)$ and $R_{rs}(547)$ are the at-surface remote sensing reflectance at 531 and 547 nm MODIS spectral bands. This formula was derived based on satellite data for R_{rs} and directly measured chlorophyll concentrations in the Kara Sea in 2007, 2011, and 2013–2015 (the number of measurements $N = 69$). This formula is similar to the formula by Kuznetsova et al. (2013) but differs from the latter in terms of its numerical coefficients and better corresponds to datasets with lower chlorophyll concentrations. For the above data, the mean chlorophyll concentration from the *in situ* data equalled 0.70 mg m^{-3}, that from (1) equalled 0.66 mg m^{-3}, and that from Kuznetsova et al. (2013) equalled 1.00 mg m^{-3}; the standard deviations equalled 0.34 and 0.43 mg m^{-3}, respectively.

A semi-analytical algorithm for solving the inverse problem was modified by Vazyulya et al. (2014) to calculate the spectral values of $K_d(\lambda)$. First, the CDOM absorption coefficient *ag*(443), the spectral slope *S* and the particle backscattering coefficient *bbp*(555) were retrieved by using R_{rs} values from the wavelength range ≥ 488 nm, and then Gordon's formula (Gordon, 1989) was used to calculate the spectral values of $K_d(\lambda)$. The obtained values of K_d were extrapolated to the short-wave portion of the spectrum by using the previously derived system of basic functions.

The spectral values of the surface irradiance $E_s(\lambda)$ for both the total and the direct and diffuse components for the entire visible range with steps of 20 nm were calculated by using MODIS Level 1 data and the SIO RAS (P. P. Shirshov Institute of Oceanology Russian Academy of Science) algorithm (Kopelevich et al., 2003). Then, the K_d_PAR for the near-surface layer, which corresponds to a level of 0.1 Es_PAR, was calculated by using the obtained values of $K_d(\lambda)$ and $E_s(\lambda)$.

As noted in previous works, the PAR model for MODIS-Aqua overestimates *in situ* values (Frouin et al., 2012). An analysis of the Kara Sea PAR dataset also shows the systematic overestimation of satellite-derived values (PAR_{sat}) compared to measured values (PAR_{meas}). On average, the PAR_{meas}/PAR_{sat} ratio equalled 0.64 ($N = 30$; $cv = 20\%$). We used this coefficient as the conversion factor of PAR_{sat} in IPP_{mod} calculations based on this empirical relationship.

2.4. IPP model validation

The models were verified by using an independent database. Notably, verification against *in situ* data that were used in model parameterization can lead to anticipatory conclusions regarding the model's performance (Behrenfeld et al., 2002). The relationships between the measured and modelled IPP estimates were tested by using linear regression. The variance of the dependent values was defined by the coefficient of determination (R^2). The slope and intercept of the linear regression determined the fitted line according to a 1:1 agreement.

The formulations that were used to calculate the model performance indices are presented in the Supplementary material (S3). The root-mean-square difference (RMSD) was used to assess the model's performance. The RMSD revealed differences between the log-transformed measured and modelled values and comprised both bias (systematic

Table 1
The main variables and definitions used in the article.

Variable	Units	Definition
IPP_{meas}	mg C m^{-2} d^{-1}	Measured depth-integrated primary production
IPP_{mod}	mg C m^{-2} d^{-1}	Modelled depth-integrated primary production
PP_z	mg C m^{-3} d^{-1}	Measured primary production at the depth z
PP_{max}	mg C m^{-3} d^{-1}	Maximum primary production value within water column
Chl_0	mg m^{-3}	Surface chl a concentration
Chl_z	mg m^{-3}	Chl a at the depth z
Chl_{max}	mg m^{-3}	Maximum chl a concentration within water column
Chl_{rel}		Relative chl a concentration within water column (Chl_z/Chl_{max})
Chl_{meas}	mg m^{-3}	Measured chl a concentration
Chl_{mod}	mg m^{-3}	Modelled chl a concentration
$\overline{Chl_{meas}}$	mg m^{-3}	Averaged within photosynthetic layer chl a concentration
$\overline{Chl_{mod}}$	mg m^{-3}	Averaged within photosynthetic layer chl a concentration calculated by model
Chl_{ph}	mg m^{-2}	Photosynthetic layer integrated chl a
k		Index of chl a vertical distribution (Chl_{ph}/Chl_0)
P^b	mg C (mg chl a)$^{-1}$ h^{-1}	Chlorophyll specific carbon fixation rate measured in ICES incubator
P^b_{opt}	mg C (mg chl a)$^{-1}$ h^{-1}	Maximum chlorophyll specific carbon fixation rate within a water column
P^b_z	mg C (mg chl a)$^{-1}$ h^{-1}	Chlorophyll specific carbon fixation rate at the depth z
P^b_{rel}		Relative chlorophyll specific carbon fixation rate ($P^b_z/P^b{}_{opt}$)
P^b_{meas}	mg C (mg chl a)$^{-1}$ d^{-1}	Measured daily chlorophyll specific carbon fixation rate within a water column
P^b_{mod}	mg C (mg chl a)$^{-1}$ d^{-1}	Modelled daily chlorophyll specific carbon fixation rate within a water column
ψ	g C (g chl a)$^{-1}$ mol quanta^{-1} d^{-1}	Water column efficiency of photosynthesis
I_0 (PAR)	mol quanta m^{-2} d^{-1}	Subsurface photosynthetically available radiation
I_z (PAR)	Relative units	Photosynthetically available radiation at the depth z
Z_{ph}	m	Photosynthetic layer up to the compensation depth
Z_s	m	Secchi disk depth
T_0	°C	Surface temperature
K_d	m^{-1}	Diffuse attenuation coefficient for downwelling irradiance
ζ		Optical depth (K_d z)

Symbols	Definition
PP	Primary production
IPP	Depth-integrated primary production
chl a	Chlorophyll a

Definiti-on	Abbreviation
RSM	Region-specific models
NRSM	Non-region specific models
PAR	Photosyntetically available radiation
UML	Upper mixed layer
SCM	Subsurface chl a maximum
CDOM	Colour dissolved organic matter
POM	Particular organic matter
DIM	Depth-integrated models
DRM	Depth-resolved models

error) and variability (σ – random error) (Doney et al., 2009; Stow et al., 2009). The log-normalized RMSD has been used to assess the overall model performance in PPARR studies (Campbell et al., 2002; Friedrichs et al., 2009; Y. Lee et al., 2015; Saba et al., 2010, 2011). Models with lower RMSD have a higher skill and *vice versa*. RMSD values close to 0.3 indicate model over- or underestimation by a factor of 2. We calculated the mean bias (B) of each model (S3) to assess over- or underestimated IPP (IPP_{meas}).

The model performance can be shown as a single plot by using a target diagram (Jolliff et al., 2009). A target diagram illustrates the total RMSD as the distance from the origin, with B on the y axis and the unbiased root-mean-square difference (uRMSD) on the x axis. Models with standard deviations that overestimate the observed σ are plotted on the right side of the diagram, and models with σ that underestimate the observed standard deviation are plotted on the left. Thus, a target diagram shows how much the model over- or underestimates the mean and variability of PP. The bias and uRMSD are normalized by σ and plotted relative to a circle with a radius of 1 (normalized σ), which illustrates whether a model performs better than the mean of the observations. Models that are located inside the circle have positive model efficiency (ME) (Stow et al., 2009). If ME $<$ 0, the mean of the observations provides a better approximation than the prediction by the model. This result suggests that the algorithm is of limited use.

3. Results

3.1. Results of region-specific IPP model development

3.1.1. Model developed by average PP, Chl a and PAR (Ψ_MOD)

A brief model description is presented in Table 3. The Kara Sea Ψ_MOD was developed by using the basin average efficiency of the irradiance utilization by the phytoplankton in the water column

Table 2
The average trophic level values of the primary productivity and abiotic parameters in the Kara Sea.

Parameter[a]	Trophic status[b]			
	0.1–0.5	0.5–1.0	1.0–2.0	> 2.0
Chl_0	0.37 ± 0.1 25	0.74 ± 0.12 30	1.35 ± 0.21 36	3.39 ± 1.13 20
Chl_{ph}	13.05 ± 6.53 21	11.57 ± 6.69 22	12.56 ± 6.88 24	30.40 ± 14.90 17
IPP_{meas}	40 ± 23 21	43 ± 36 22	60 ± 46 24	142 ± 109 17
P^b_{opt}	1.03 ± 0.57 21	1.09 ± 1.89 22	0.96 ± 0.60 24	1.21 ± 0.61 17
Z_{ph}	38 ± 23 21	20 ± 7 22	14 ± 8 24	12 ± 5 17
ψ	0.57 ± 0.39 22	0.68 ± 0.42 16	0.88 ± 0.75 15	0.90 ± 0.61 16
K_d	0.210 ± 0.147 25	0.308 ± 0.062 30	0.447 ± 0.129 36	0.582 ± 0.132 19
I_0	7.32 ± 4.43 23	4.16 ± 2.53 16	4.60 ± 3.48 15	8.86 ± 8.07 16
UML	10 ± 5 25	8 ± 4 30	7 ± 3 36	10 ± 7 20
k	41.73 ± 28.32 21	16.3 ± 79.65 22	9.40 ± 5.23 24	8.93 ± 2.92 17

[a] Average values and standard deviation (± σ) are represented above the line and number of the data below the line.
[b] Waters of different trophic status were separated according to values of Chl_0 (mg m^{-3}).

Table 3
Models description and data sources.

Abbreviation	Definition	Model type	Input data for model validation and type of the data	Sources	Model adaptation (region of development)
SCHL_reg	Algorithm that was based on empirical relation among surface chl *a* and IPP	DIM	Chl_0 *in situ*	This article	Kara Sea (RSM)
Ψ_MOD	Model that was developed by average PP, chl *a* and PAR	DIM	Chl_0, PAR *in situ*	This article	Kara Sea (RSM)
VGPM	Vertically Generalized Production Model	DIM	Chl_0, $P^b{}_{opt}$, Z_{ph}, PAR *in situ*	Behrenfeld and Falkowski, 1997a	World Ocean (NRSM)
VGPM_Arc	VGPM that was modified by Arctic $P^b_{opt} - T_0$ relationship	DIM	Chl_0, T_0, PAR *in situ*	Behrenfeld and Falkowski, 1997a; Cota et al., 2004	World Ocean (NRSM)
VGPM_TR	VGPM that was modified by averaged P^b_{opt} in the different Kara Sea trophic regions (TR)	DIM	Chl_0, $P^b{}_{opt}$, PAR *in situ*	Behrenfeld and Falkowski, 1997a, 1997b; this article	World Ocean (NRSM)
ZCHL_reg	Model that was based on empirical relation among Kara Sea Chl_z and PP_z	DRM	Chl_z *in situ*	This article	Kara Sea (RSM)
KSDRM	Kara Sea depth-resolved model	DRM	Chl_0, PAR, K_d *in situ*	This article	Kara Sea (RSM)
ArcPP	Model that was based on empirical relation among Arctic Ocean Chl_z and PP_z	DRM	Chl_z *in situ*	Hill et al., 2013	Arctic Ocean (NRSM)
Ψ_MOD$_{sat}$	Model that was developed by average PP, chl *a* and PAR	DIM	Chl_0, PAR satellite-derived	This article	Kara Sea (RSM)
KSDRM$_{sat}$	Kara Sea depth-resolved model	DRM	Chl_0, PAR, K_d satellite-derived	This article	Kara Sea (RSM)

($\psi = P^b_{meas}/I_0$) (Falkowski, 1981) and the index of the vertical chl *a* distribution ($k = Chl_{ph}/Chl_0$) (Campbell et al., 2002) as the model coefficients. The input variables were the surface chl *a* and daily incident solar radiation (PAR), parameters that can be easily measured in the field. Thus, the primary production in the water column can be calculated as follows:

$$IPP_{mod} = k\ \psi\ Chl_0\ I_0 \tag{2}$$

Previously, this model was tested in the PPARR2 (Campbell et al., 2002) and was applied to investigate the PP spatial variability in the Drake Passage (Demidov et al., 2011). In the framework of the presented study, we calculated the average $k\ \psi$ value as the Kara Sea region-specific coefficient. The geometric average of $k\ \psi$ was applied consistently with its log-normal frequency distribution (Fig. 3) (Aitchison and Brown, 1957). The geometric average of the Kara Sea $k\ \psi$ equalled 8.27:

$$IPP_{mod} = 8.27\ Chl_0\ I_0 \tag{3}$$

3.1.2. Parameterization of the vertical profiles of chlorophyll distribution and its use in the Kara Sea depth-resolved model (KSDRM)

The KSDRM was developed by using the maximal chlorophyll specific photosynthetic rate within the water column (P^b_{opt}), underwater assimilation activity and vertical profiles of the chl *a* distribution. A conceptual formula of the IPP calculation is presented below:

$$IPP = \int_z^0 P^b_z\ Chl_z\ DL\ (dz) \tag{4}$$

where $P^b{}_z$ is the chlorophyll specific carbon fixation rate at depth z, Chl_z is the chl *a* content at depth z and DL is the day length.

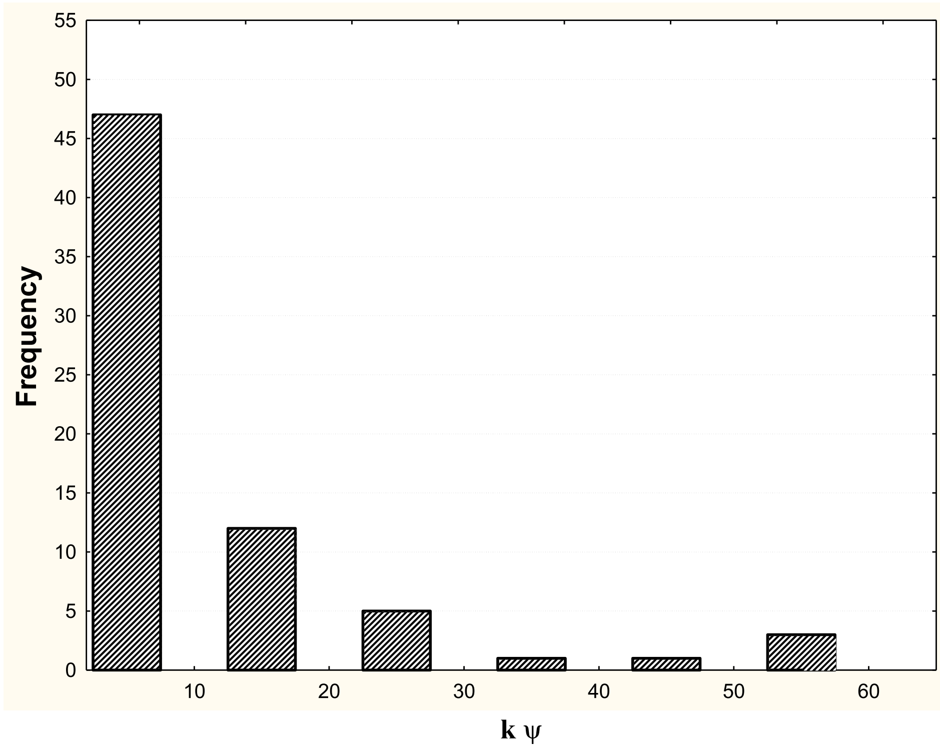

Fig. 3. Frequency distribution of the Ψ_MOD coefficient $k\ \psi$ (model description see in the Table 3 and in the text of the article).

Modelled values of P^b_z were calculated based on the power dependence of $P^b{}_{rel}$ ($P^b{}_z/P^b{}_{opt}$) values on the relative PAR I_z (% I_0) (Fig. 4):

$$P^b_{rel} = 11.65\ I_z^{0.49} \tag{5}$$

hence,

$$P^b{}_z = (P^b{}_{opt}(11.65\ I_z^{0.49}))/100 \tag{6}$$

The maximum water column chlorophyll specific carbon fixation rate (P^b_{opt}) was obtained from the empirical relationship between $P^b{}_{opt}$ and I_0, which was recently calculated by Demidov et al. (2014):

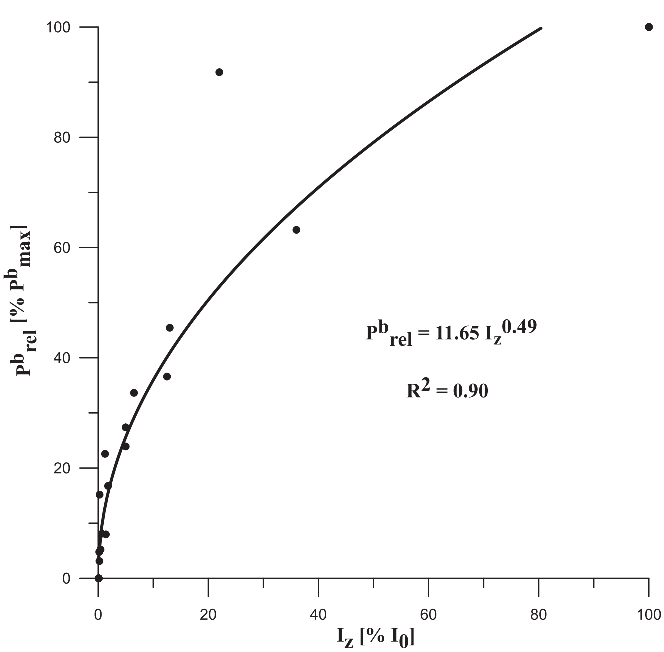

Fig. 4. Average values (in relative units) of chlorophyll specific carbon fixation rate (P^b_{rel}) *vs.* average relative values of subsurface PAR at depth z (I_z).

$$P^b_{opt} = 10^{-0.71+0.90\ \log_{10} I_0} \tag{7}$$

By substituting formula (7) into Eq. (6), P^b_z can be calculated as follows:

$$P^b{}_z = ((10^{-0.71+0.90\ \log_{10} I_0})(11.65\ I_z^{0.49}))/100 \tag{8}$$

The next step in the KSDRM's development is the calculation of the chl *a* concentration at each depth (Chl_z) by using Chl_0. Previous studies noted that the shape of the vertical chl *a* curve depends on Chl_0 and, consequently, on the trophic status of the region (Morel and Berthon, 1989; Uitz et al., 2006). Five-meter averages of vertical chl *a* profiles were created within the upper 55-m layer for each trophic category (Fig. 5). Every individual profile was normalized to the maximum chlorophyll value (Chl_z/Chl_{max}) to overcome the non-normal chl *a* distribution within each depth bin and to illustrate the relative vertical chlorophyll pattern. The distribution of the normalized curves was considered relative to the optical depth $\zeta = z\ K_d$, where z is the geometric depth and K_d is the diffuse attenuation coefficient for downwelling irradiance. Then, the obtained profiles were mathematically approximated.

As seen in Fig. 5, the average normalized vertical chl *a* profiles were linearly approximated with high determination coefficients ($R^2 = 0.65$–0.96) in the waters of trophic categories I and IV and exponentially ($R^2 = 0.92$ and 0.93) in the waters of trophic categories II and III. In the category I waters, the curves within and below the euphotic layer (1% PAR) were approximated separately (Fig. 5). Interestingly, the chl *a* concentrations permanently decreased with depth for $Chl_0 > 0.5\ \mathrm{mg\ m^{-3}}$. A homogenous chlorophyll distribution within the euphotic layer and a linear decrease below this layer were observed with relatively low Chl_0 (0.1–0.5 mg m^{-3}). Registering Chl_{max} at the surface or within the subsurface layer, *i.e.*, $Chl_{max} \approx Chl_0$, is the principle for applying vertical chl *a* profiles in the KSDRM.

The chlorophyll content at each depth (Chl_z) can be calculated by using the equations which are given in the Supplementary material (S4). Thus, we can calculate IPP_{mod} at each site within waters of different trophic status by substituting Eq. (8) and the Chl_z calculation

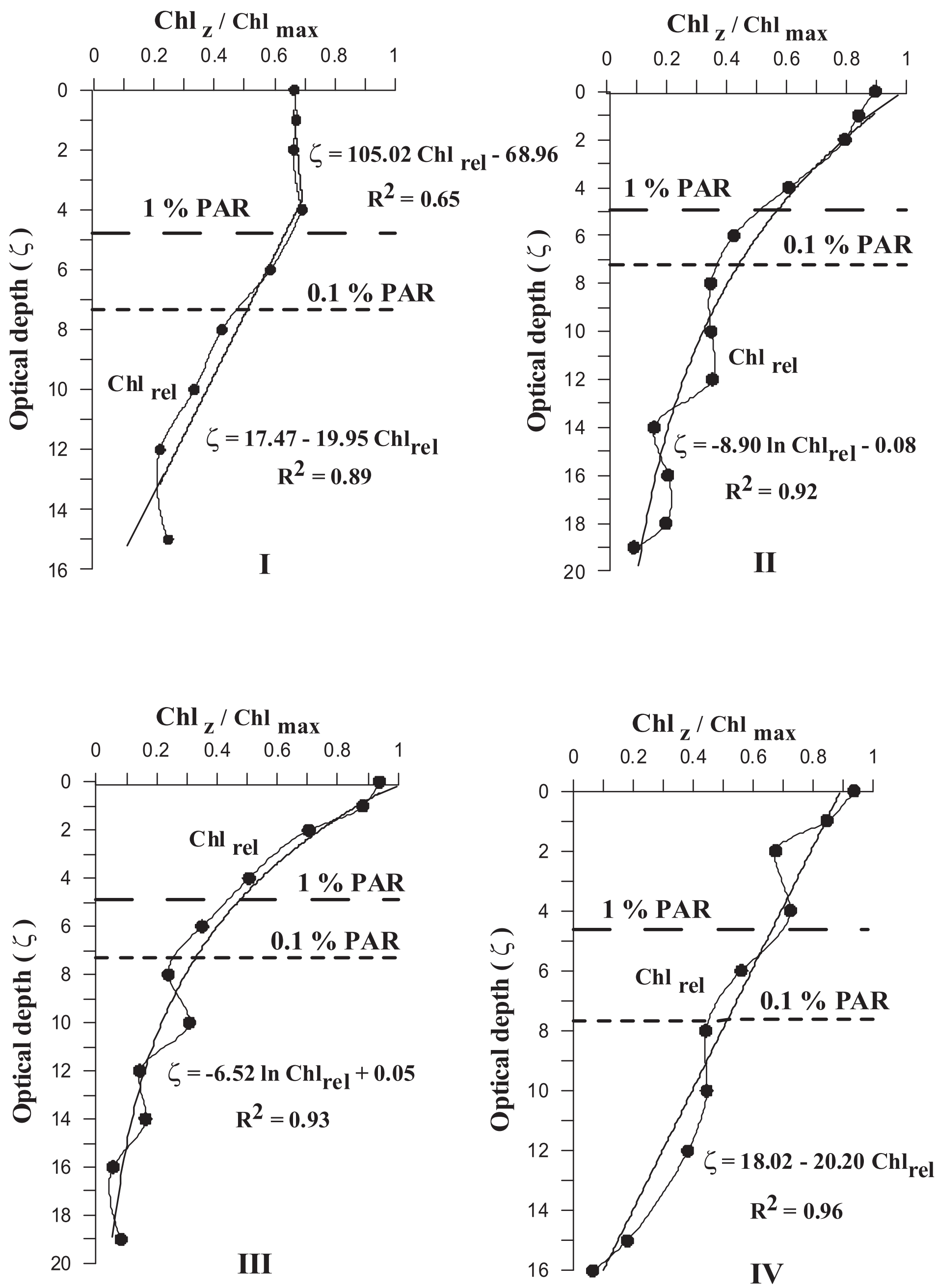

Fig. 5. Relationships among average chl *a* relative values ($Chl_{rel} = Chl_z/Chl_{max}$) and optical depths ($\zeta$) in the Kara Sea waters of different trophic status defined according to surface chl *a* concentration (Chl_0): I – Chl_0 ranged from 0.1 to 0.5 mg m^{-3}; II – Chl_0 ranged from 0.5 to 1.0 mg m^{-3}; III – Chl_0 ranged from 1.0 to 2.0 mg m^{-3}; IV – $Chl_0 > 2.0$ mg m^{-3}. Horizontal lines are presented 1% and 0.1% PAR. Bold lines are fitted and dots are measured results.

(S4) into Eq. (4).

3.1.3. Empirical relationship between the Kara Sea Chl_z and PP_z (ZCHL_reg model)

The relationship between the log-transformed Kara Sea primary production and chl *a* at all depths is presented in Fig. 6a. The equation of linear regression is

$$\log_{10}PP_z = 0.43 + 1.13\ \log_{10} Chl_z (R^2 = 0.27; N = 355; p < 0.01) \quad (9)$$

This formula was applied to calculate the depth-resolved PP by using model curves of chl *a*'s vertical distribution. An analogous approach with the ARCSS-PP dataset has been applied by Hill et al. (2013) for Arctic Ocean IPP estimation.

3.2. Algorithm skill assessment with field data

3.2.1. Results of regression analysis

We tested Chl-based algorithms that were developed based on the Kara Sea dataset, *i.e.*, region-specific models (RSM), by using field observations. The skill assessment of these algorithms was compared to that of non-region-specific algorithms (NRSM) (Behrenfeld and Falkowski, 1997a; Hill and Zimmerman, 2010). The results of the regression analysis (Fig. 7; Table 4) suggest that all the models predicted from 47 to 93% of the *in situ* IPP. The analysed algorithms were divided into five groups in terms of their coefficient of determination as an indicator of model predictive capacity. Models that were developed solely based on the chl *a* distribution within the water column (Chl_z) (ZCHL_reg and ArcPP) (Table 3) had the least predictive skill (R^2 = 0.40–0.50). The second category (R^2 = 0.50–0.60) included

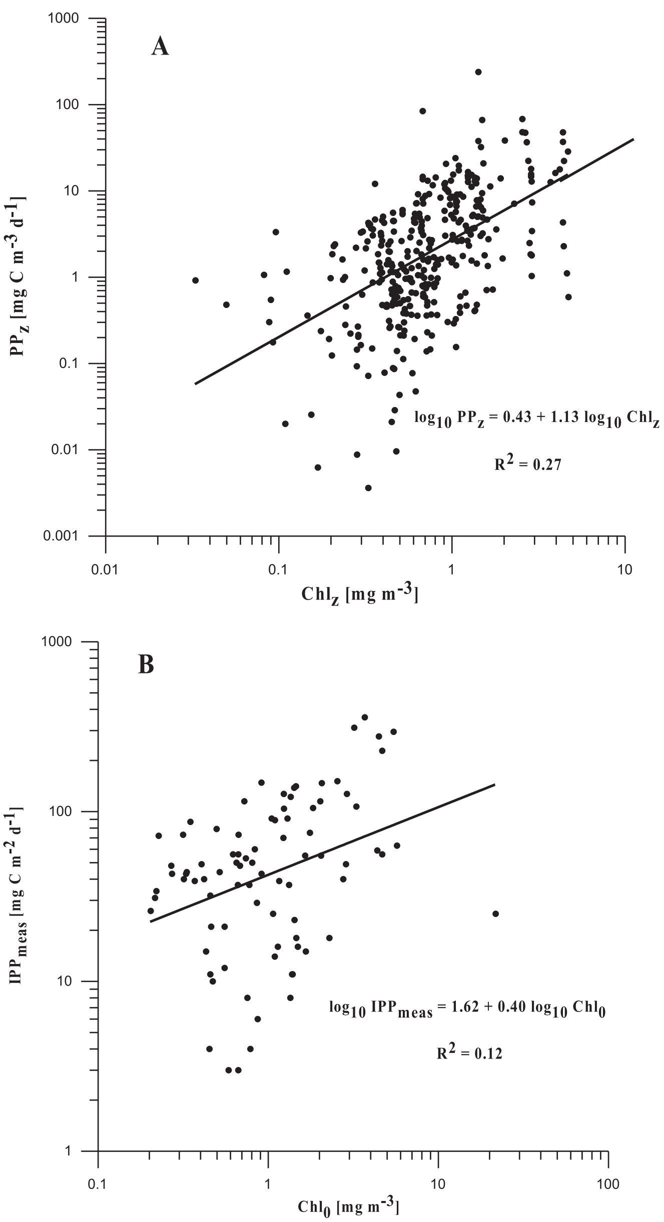

Fig. 6. (A) – primary production (PP_z) *vs.* chl *a* (Chl_z) for all depths and (B) – depth-integrated primary production (IPP_{meas}) *vs.* surface chl *a* concentration (Chl_0).

two modified VGPM types, which comprised (i) P^b_{opt}, which was calculated by the regional temperature relationship (VGPM_Arc), or (ii) the average P^b_{opt} (VGPM_TR). Better performance was observed for the regional IPP algorithms SCHL_reg and Ψ_MOD (third category) (R^2 = 0.60–0.70) and the depth-resolved KSDRM (fourth category) (R^2 = 0.70–0.80). The best performance ($R^2 > 0.90$) (fifth category) was observed for the VGPM with the *in situ* P^b_{opt} as an input variable (Table 4).

A perfect algorithm in terms of regression analysis has a 1:1 relationship between the predicted and observed PP (slope = 1). The lowest value of the slope (0.40) was calculated for the simple model that was based on Chl_0 (SCHL_reg) (Fig. 7a). The best relationship between IPP_{mod} and IPP_{meas} was observed for Ψ_MOD (slope = 0.98) (Fig. 7b) and VGPM (slope = 1.02) (Fig. 7g). A relatively high slope was calculated for the KSDRM (slope = 0.74) (Fig. 7d). The relationships between the predicted and observed IPP for the other algorithms ranged from 0.54 to 0.62 (Table 4).

3.2.2. RMSD, model efficiency (ME), biases and variance

The RMSD and ME values are represented in Table 4 and Fig. 8. In terms of the individual model skill, the region-specific algorithms that were developed by using photoadaptive parameters (Ψ_MOD and KSDRM), along with the VGPM (*in situ* P^b_{opt} as the input variable) (RMSD ranged from 0.27 to 0.31), had the best predictive capacity. The models that only considered the chlorophyll concentration (as an index of phytoplankton biomass) (SCHL_reg and ZCHL_reg), along with the modified VGPM and ArcPP, performed worse (RMSD ranged from 0.32 to 0.59). The same result was found when the ME was considered as a performance index. NRSM ArcPP and VGPM_Arc had the least skill (RMSD equal to 0.59 and 0.54, respectively) and ME < 0 (Fig. 8; Table 4).

We used a target diagram to illustrate the capacity of the models to estimate IPP better than the average value (Fig. 9). Symbols inside the circle (normalized standard deviation of the *in situ* IPP) indicate better performance *versus* the mean field data. As seen in Fig. 9, only two models (ZCHL_reg and Ψ_MOD) underestimated the *in situ* depth-integrated PP. Additionally, all the algorithms overestimated the IPP variability. Thus, the modelled standard deviation exceeded the observed standard deviation. The performance indices in Table 4 also suggest that the region-specific models (SCHL_reg, Ψ_ MOD and KSDRM) had the fewest biases.

3.2.3. Simulated vertical chl a distribution and assimilation activity in the depth-resolved algorithm (KSDRM)

Simulated vertical chl *a* profiles were compared with the *in situ* chl *a* distribution in waters of different trophic status and are given in the Supplementary material (S5 and S6). Significant variability was present in the form of *in situ* chl *a* curves. The subsurface chlorophyll maximum

Table 4
Regression statistics, performance indices for the log-transformed IPP_{meas} and IPP_{mod} and average values (mg C m^{-2} d^{-1}) for the each model type.

Model type	Averaged IPP_{mod}[a]	Regression statistics				Performance indices				
		Slope	Intercept	R^2	*p* value	*B*	*σ*	RMSD	uRMSD	ME
SCHL_reg	58 ± 38	0.40	1.05	0.65	< 0.01	0.07	0.23	0.32	0.31	0.53
Ψ_MOD	90 ± 130	0.98	0.01	0.69	< 0.01	− 0.03	0.56	0.31	0.30	0.58
VGPM	141 ± 175	1.02	0.21	0.93	< 0.01	0.24	0.50	0.27	0.13	0.66
VGPM_Arc	196 ± 188	0.59	1.19	0.60	< 0.01	0.51	0.36	0.59	0.30	− 0.60
VGPM_TR	104 ± 106	0.62	0.84	0.58	< 0.01	0.21	0.39	0.37	0.31	0.37
ZCHL_reg	33 ± 29	0.55	0.48	0.50	< 0.01	− 0.25	0.37	0.42	0.33	0.21
KSDRM	99 ± 113	0.74	0.59	0.74	< 0.01	0.17	0.41	0.29	0.24	0.62
ArcPP	160 ± 163	0.54	1.17	0.47	< 0.01	0.42	0.37	0.54	0.34	− 0.34
Average IPP_{meas}[a]	77 ± 94									

Slope and intercept – parameters of linear regression; R^2 – coefficient of determination; *p* value indicates the significance level of each regression. Indices are mean model bias (*B*), standard deviation (*σ*), root-mean-square-difference (RMSD), unbiased root-mean-square-difference (uRMSD) and model efficiency (ME).
[a] Mean values and standard deviation are presented (N = 31).

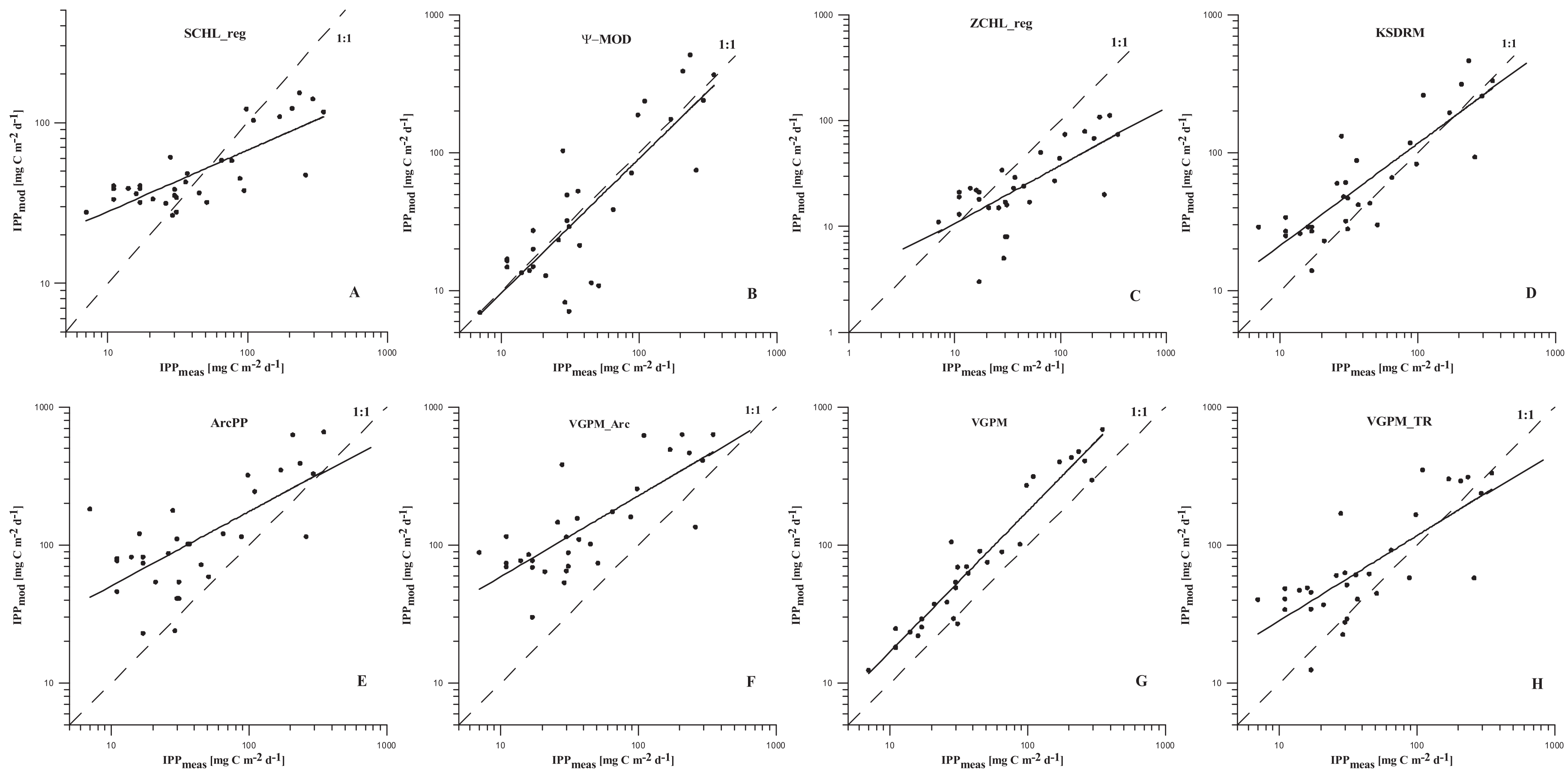

Fig. 7. Comparison of measured (IPP_{meas}) and modelled (IPP_{mod}) depth-integrated values of primary production that were calculated by different algorithms: (A) – model that was based on relationship between surface chl *a* and IPP_{meas}; (B) – model that was developed by using average Kara Sea data (Ψ_MOD); (C) – model that was based on relationship among Chl_z and PP_z; (D) – Kara Sea depth-resolved model; (E) – model that was based on relationship among Arctic Ocean Chl_z and PP_z (Hill et al., 2013); (F) – VGPM modified by using Arctic Ocean $P^b_{opt} - T_0$ relationship; (G) – VGPM; (H) – VGPM modified by using average P^b_{opt} in the different Kara Sea trophic regions (TR) (model descriptions see in the Table 3).

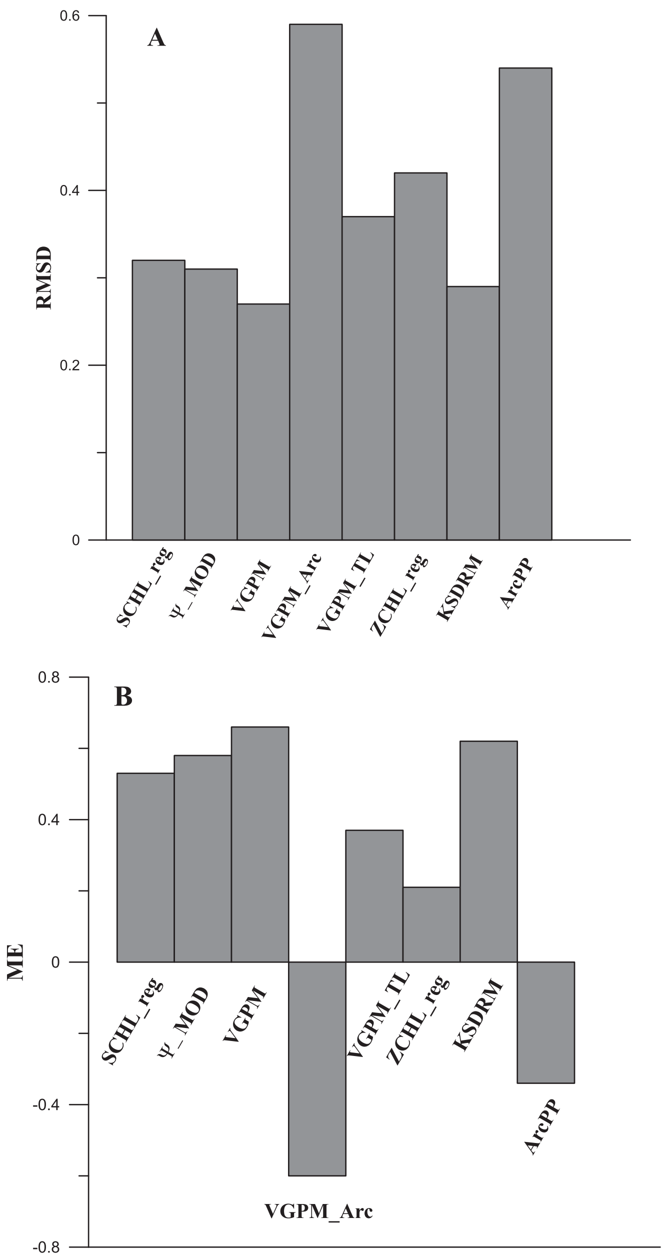

Fig. 8. Root-mean-square difference (RMSD) (A) and model efficiency (ME) of different Kara Sea models.

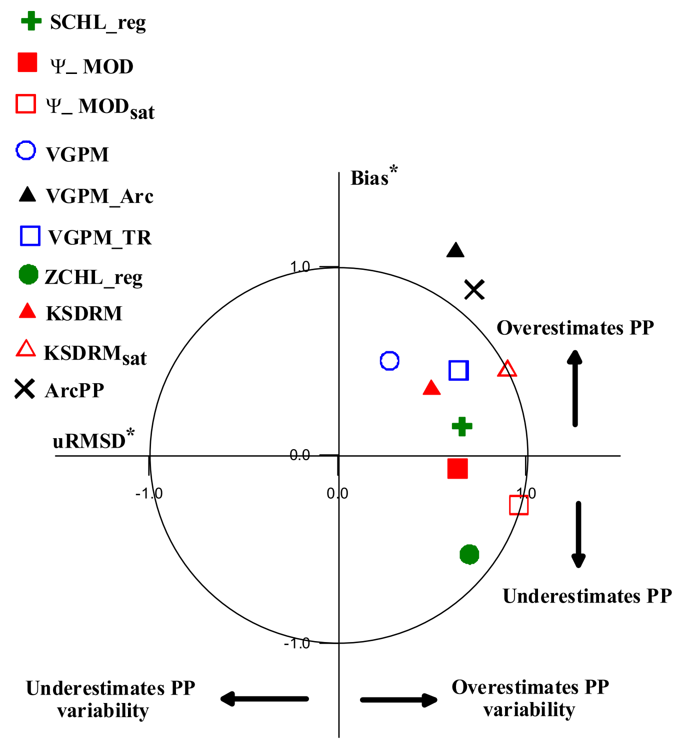

Fig. 9. Target diagram for the individual models. Bias* and uRMSD* are normalized B and uRMSD by using standard deviation of log-transformed IPP_{meas}. The solid circle is the normalized standard deviation of the log-transformed IPP_{meas} (σ = 0.477).

(SCM) was a common feature of the vertical chl *a* distribution in the waters of trophic category I (Chl_0 ranged from 0.1 to 0.5 mg m^{-3}) (S5). The presence of the SCM led to the divergence of the modelled and observed vertical chl *a* profiles. Conversely, no pronounced SCM was observed in the waters of categories II–IV (S6). A comparison of the modelled and observed profiles suggests that the predicted vertical distribution usually underestimated the *in situ* concentration in the top of the euphotic zone and often overestimated chl *a* below this layer (S5 and S6).

Evaluating the contributions of the chl *a* concentration and phytoplankton assimilation activity within the water column in the overall error of the IPP determination is important. Fig. 10a illustrates that the modelled chl *a* within the photosynthetic layer, which was expressed as the mean concentration ($\overline{Chl_{mod}}$), relatively satisfactorily predicted the observed values ($\overline{Chl_{meas}}$) (R^2 = 0.90; RMSD = 0.21). On the contrary, weak correlation existed between the simulated following Eq. (5)–(8) and measured water column daily assimilation activity (R^2 = 0.42; RMSD = 0.43) (Fig. 10b). These results indicate a significant role of the accuracy in the determination of the chlorophyll-specific carbon fixation rate (P_z^b) for the depth-resolved IPP algorithms.

3.3. Skill assessment of region-specific algorithms with satellite data as input variables

In this section, we compare the performance of region-specific algorithms with satellite-derived (Ψ_MOD$_{sat}$ and KSDRM$_{sat}$) and *in situ* data as input variables (Table 3). The satellite-derived chl *a* (Chl_{sat}) is the concentration within the penetration depth ($1/K_d$). Regression analysis suggested that the average chl *a* in the Kara Sea average within the penetration depth was strongly correlated with Chl_0 (R^2 = 0.99; slope = 0.98; N = 104) (Demidov et al., 2014).

The performance of Ψ_MOD$_{sat}$ in terms of the RMSD did not vary with the application of Chl_{sat} from the region-specific algorithm and MODIS-Aqua PAR as input variables. On the other hand, the R^2 and ME values decreased by a factor of 3.1 and 4.5, respectively (Tables 5 and 6 and Fig. 11). Ψ_MOD$_{sat}$, similar to Ψ_MOD, underestimated IPP_{meas} (B = −0.08).

Interestingly, almost no differences were observed in the model predictive capacity between the KSDRM and KSDRM$_{sat}$ in terms of the RMSD (0.31 and 0.29, respectively) and B (0.14 and 0.17, respectively) (Tables 4 and 5 and Fig. 11). On the other hand, the R^2 of KSDRM$_{sat}$ decreased by a factor of 2.7 compared to the KSDRM.

Comparing the predictive skill of the DIM (Ψ_MOD$_{sat}$) and DRM (KSDRM$_{sat}$) is interesting. The regression statistics and performance indices, which are presented in Table 5, suggest that the differences in the model predictive capacity between Ψ_MOD$_{sat}$ and KSDRM$_{sat}$ are negligible. Thus, KSDRM$_{sat}$ and Ψ_MOD$_{sat}$ performed equally when satellite data were used as input variables.

4. Discussion

In this study, we presented the development of a Kara Sea regional

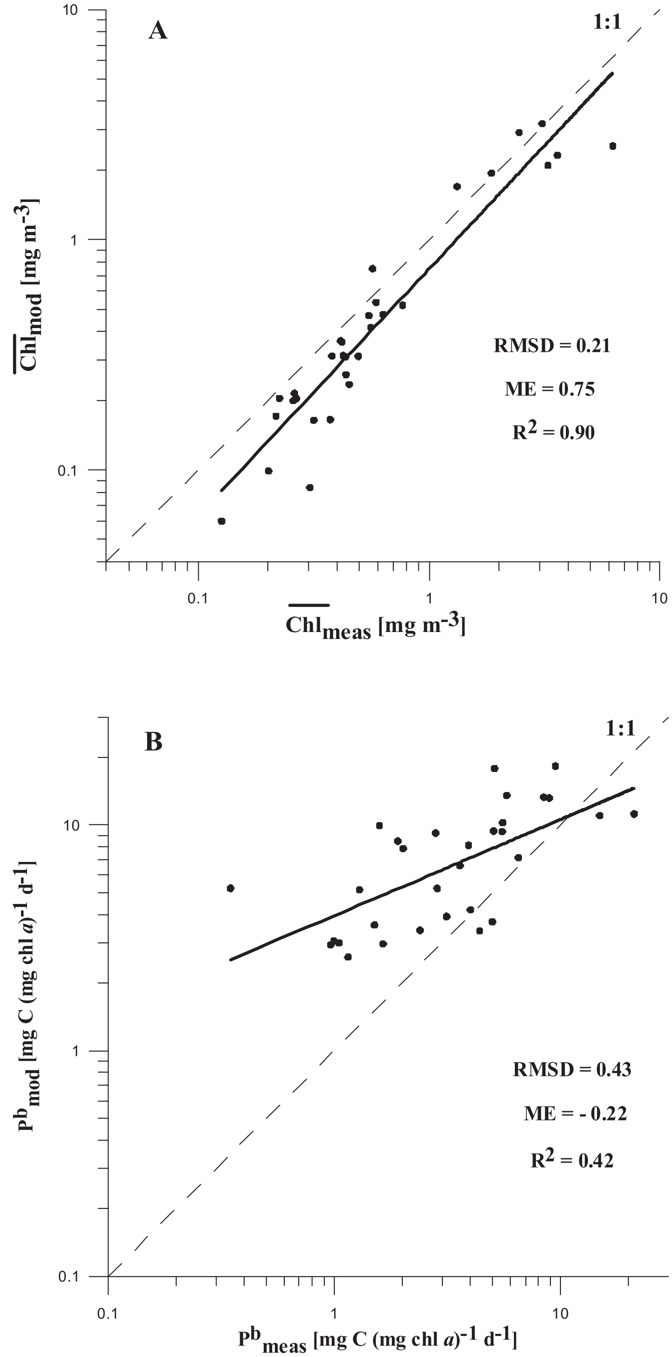

Fig. 10. (A) – comparison of measured ($\overline{Chl_{meas}}$) and modelled ($\overline{Chl_{mod}}$) chl *a* concentration averaged within photosynthetic layer; (B) – comparison of measured (P^b_{meas}) and modelled (P^b_{mod}) daily chlorophyll specific carbon fixation rate within a water column.

models and a comparison of the predictive skills of different algorithms. Below, we discuss the model skill of the depth-integrated, depth-resolved, simple and more complex algorithms. Additionally, the RSM and NRSM are compared.

4.1. Comparison of the DIM and DRM algorithms

A comparative analysis of the model skill in terms of the regression statistics and performance indices implies that the differences in the predictive capacity of the Kara Sea depth-resolved and depth-integrated algorithms were insignificant (Table 4). The negligible differences in the performance between the DIM (Ψ_MOD) and DRM (KSDRM) were consistent with Behrenfeld and Falkowski (1997a, 1997b), who concluded that the application of vertical chl *a* profiles did not significantly improve IPP estimation. Following these authors, the DIM algorithms explained ~85% of the IPP variability, while only ~15% of the variance could be explained by the vertical distribution of chl *a* and PAR. The results of the Kara Sea RSM development suggest that the vertical resolution increased the model performance in terms of the RMSD and ME by only ~7% (Table 4). Regarding the patterns of the Kara Sea primary production characteristics, a minor difference between Ψ_MOD and KSDRM can be attributed to the strong contribution of surface PP to the IPP, the small photosynthetic layer and weak SCM development in most regions (Demidov and Mosharov, 2015). The chlorophyll distribution pattern was characterized, on average, by a maximum at the surface and linear or exponential decay with depth (Fig. 5). The contribution of the SCM's development, presumably in the category I waters, to the IPP was insignificant and ranged from 1 to 27% (Demidov et al., 2014). It is worth to note that vertical chl *a* distribution pattern during autumn presented in this article is consistent with the annual mean profile in the Kara Sea from the ARCSS-PP database (Arrigo and van Dijken, 2011). On the other hand, we realise that the Kara Sea vertical chlorophyll distribution dataset is restricted by autumn and number of profiles (N = 107). Currently, we cannot go to the final conclusion about role of the vertical chlorophyll distribution in the Kara Sea primary production. Scarcity of the Kara Sea data is especially evident in comparison with other datasets that were used to describe the typical chlorophyll profiles in the different regions of the World Ocean: 5206 profiles (Ardyna et al., 2013), 1199 profiles (Cherkasheva et al., 2013), 4000 profiles (Morel and Berthon, 1989), 2419 profiles (Uitz et al., 2006).

The presented curves of the vertical chl *a* distribution in the Kara Sea are distinguished from those in Arctic Ocean PP models. Typically, the vertical chl *a* distribution is described as homogenous within the UML and is assumed to exponentially decrease downward (Arrigo et al., 2008; Pabi et al., 2008). A similar picture for post-bloom conditions was considered by Hill and Zimmerman (2010) in the Chukchi Sea. The homogenous chlorophyll distribution from the surface to the base of the euphotic zone was considered by these authors during the pre-bloom period. A constant chl *a* concentration throughout the depth of integration was used later for *in situ* and remotely sensed IPP estimations in the Arctic Ocean (Hill et al., 2013).

Unlike in the Kara Sea, the SCM is a common feature of the vertical water column structure in the Arctic Ocean (Brown et al., 2015;

Table 5
Results of region-specific Kara Sea model validation with MODIS-Aqua data. Regression statistics and performance indices for the log-transformed IPP_{meas} and IPP_{mod} are presented.

Model type	Regression statistics					Performance indices				
	Slope	Intercept	R^2	N	p value	B	σ	RMSD	uRMSD	ME
Ψ_MOD$_{sat}$	0.42	1.02	0.22	26	0.02	− 0.08	0.27	0.30	0.29	0.13
KSDRM$_{sat}$	0.44	1.19	0.27	26	0.01	0.14	0.26	0.31	0.27	− 0.06

Ψ_MOD$_{sat}$ and KSDRM$_{sat}$ – depth-integrated and depth-resolved Kara Sea region-specific models with satellite data as input variables. Slope and intercept – parameters of linear regression; R^2 – coefficient of determination; p value indicates the significance level of each regression. Indices are mean model bias (B), standard deviation (σ), root-mean-square-difference (RMSD), unbiased root-mean-square-difference (uRMSD) and model efficiency (ME).

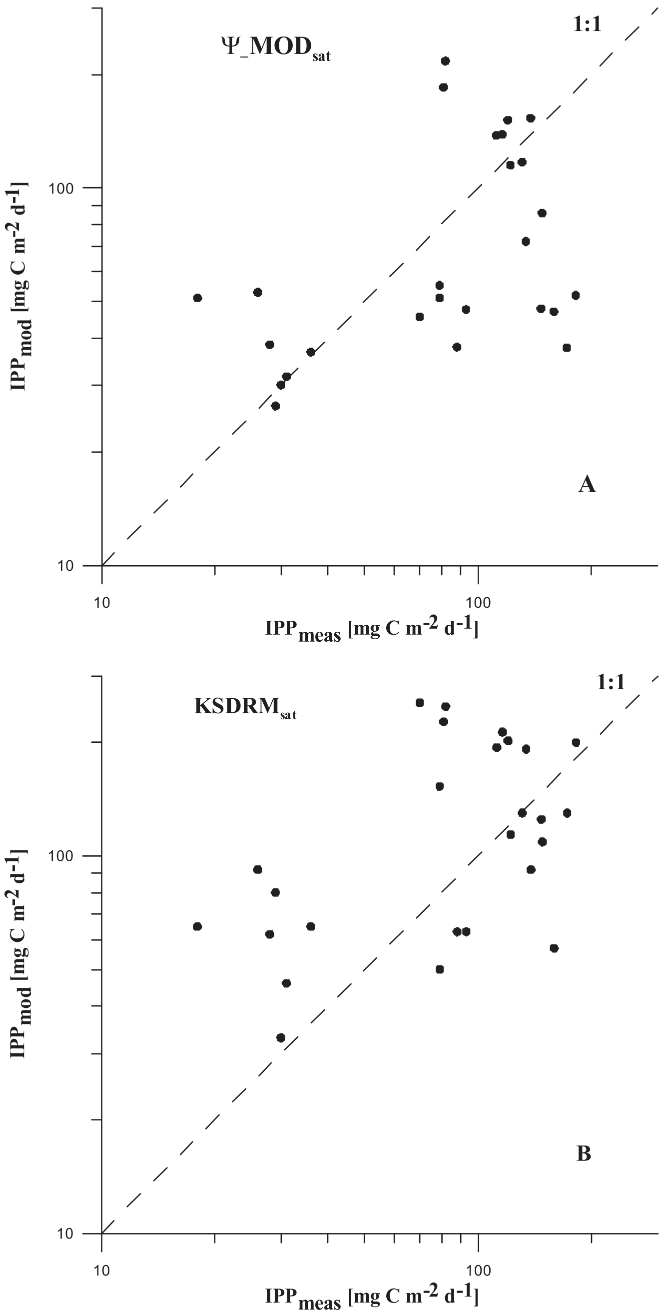

Fig. 11. Comparison of measured (IPP_{meas}) and modelled (IPP_{mod}) depth-integrated values of primary production that were calculated by using region-specific models with MODIS-Aqua data (chl *a*, PAR and K_d) as input variables. A – depth-integrated Ψ_MOD; B – depth-resolved KSDRM.

Cherkasheva et al., 2013; Martin et al., 2010, 2012). The SCM mainly forms during the post-bloom period, occasionally promoting a deep primary production maximum or smoothing PP profiles and essentially determining the annual IPP (Hill et al., 2013; Zhai et al., 2012). On the other hand, other authors noted that variations in the vertical chl *a* distribution have limited effects on AO IPP (Ardyna et al., 2013; Arrigo et al., 2011; Cherkasheva et al., 2013).

4.2. Maximal water column chlorophyll specific carbon fixation rate (P^b_{opt}) in the Kara Sea IPP models

The importance of accurate P^b_{opt} estimates in IPP models is widely known (Balch and Byrne, 1994; Behrenfeld and Falkowski, 1997a), but difficulties exist in the determination of this parameter (Behrenfeld and Falkowski, 1997b). Longhurst et al. (1995) proposed P^b_{opt} as a mean value for biogeochemical provinces to resolve this problem. Another approach is to establish a relationship between P^b_{opt} and an environmental factor that limits phytoplankton assimilation activity, *e.g.*, the surface temperature (Megard, 1972; Behrenfeld and Falkowski, 1997a).

In a previous study (Demidov et al., 2014), we attempted to determine the main abiotic factor that affects P^b_{opt} in the Kara Sea. We suggested that the incident PAR strongly influenced the chlorophyll-specific carbon fixation rate during the autumn. Thus, we concluded that I_0 can be useful in the P^b_{opt} algorithm at the end of the vegetation season. Previously, Behrenfeld et al. (2002) revealed that the application of growth radiation as an input variable significantly improved photoacclimation models' predictive capacity compared to a temperature-dependent P^b_{opt} model, which constituted approximately 9% of the variance in the chlorophyll-specific carbon fixation rate. The irradiance-dependent model that was applied in our study constituted 27% of the variance in P^b_{opt}. The lack of a correlation between the measured and modelled values (Fig. 10b) provided additional evidence of the importance of P^b_{opt} algorithm enhancement.

Testing the influence of *in situ* P^b_{opt} as an input variable on model performance was also informative. Table 4 illustrates that the VGPM had optimal regression statistics (slope = 1.02; R^2 = 0.93), the lowest regression error (RMSD = 0.27) and the highest model efficiency (ME = 0.66) when the measured P^b_{opt} was used as an input variable. Additionally, previous studies have shown that using the *in situ* P^b_{opt} in the VGPM increased the model performance. Ishizaka et al. (2007) verified the predictive capacity of the VGPM with the application of field observations in Sagami Bay (Japan). The use of the *in situ* P^b_{opt} in the model formula increased R^2 from 0.43 to 0.48 compared to the original VGPM, where P^b_{opt} was calculated from the temperature dependence (Behrenfeld and Falkowski, 1997a). A better result was achieved by Isada et al. (2010) in the Oyashio region. Their application of the *in situ* P^b_{opt} in the VGPM improved the model's performance in terms of the coefficient of determination (an increase from 0.48 to 0.65). Additionally, using the *in situ* P^b_{opt} in the VGPM increased the model's predictive capacity in the Southern Ocean (Hirawake et al., 2011).

4.3. Role of incident PAR as an input variable and photoadaptive parameters as model coefficients in the improvement of region-specific models

The chl *a* concentration is considered in the simplest models as the index of water column productivity (Eppley et al., 1985; Smith and Baker, 1978). In previous studies, chl *a* was used for IPP estimates in the Arctic Ocean (Hill and Zimmerman, 2010; Hill et al., 2013; Matrai et al., 2013), the Eurasian Arctic sector (Vetrov and Romankevich, 2011), the Southern Ocean (Puigcorbé et al., 2017) and the World Ocean (Vinogradov et al., 1996).

The relationship between chl *a* and PP was found to be a simple conversion factor without involving more complex parameterization with chlorophyll specific assimilation activity and irradiance. Hill et al. (2013) found a close relationship between the log-transformed chl *a* concentration and daily PP for all depths (R^2 = 0.66) based on the ARCSS-PP dataset. These authors drew a conclusion regarding the possibility of predicting IPP without PAR and photoadaptive parameters as input variables based on these results. This conclusion was confirmed by the results of studies in the Beaufort Sea, where establishing a reliable relationship between the primary production and phytoplankton assimilation activity was not possible (Hill and Cota, 2005).

The results of our study demonstrate a minor correlation between chl *a* and PP at all depths (R^2 = 0.27) (Fig. 6a; Table 4). Additionally, the regression analysis of Chl_0 and IPP_{meas} revealed that only 12% of the variability in the Kara Sea IPP depended on the surface chl *a* (Fig. 6b; Table 4). Thus, the chl *a* concentration at the end of the vegetative season was not an index of phytoplankton productivity within the photosynthetic layer. In the World Ocean, Chl_0 defines < 50% of integrated primary production (Banse and Yong, 1990; Balch et al., 1992; Behrenfeld and Falkowski, 1997b). On the other hand, a strong correlation between IPP_{meas} and $P^b{}_{opt}$ ($R^2 = 0.64$) was established in the Kara Sea. Furthermore, IPP_{meas} and $P^b{}_{opt}$ mainly depended on PAR (Demidov et al., 2014). In the other Arctic Seas, the role of light in PP also increases at the end of the growing season (Brugel et al., 2009; Hegseth, 1997; Platt et al., 1987; Yun et al., 2012). Thus, we expected that including $P^b{}_{meas}$, ψ and I_0 in the IPP algorithms would improve the model performance.

As seen in Table 4, Ψ_MOD and KSDRM, which used P^b_{meas} and ψ as model coefficients and I_0 as an input variable, predicted IPP_{meas} better than models that were solely based on chlorophyll concentration. This statement applies to both the regression statistics and performance indices. Interestingly, SCHL_reg (a Chl_0-based model) had better predictive skill than ZCHL_reg (a Chl_z-based model). Generally, the region-specific Ψ_MOD and KSDRM algorithms performed approximately 1.5-fold better than ZCHL_reg (RMSD = 0.29, 0.31 and 0.42, respectively).

The mean model biases suggest that ZCHL_reg underestimated and SCHL_reg overestimated the observed PP values (Table 4). Previously, Hill and Zimmerman (2010) concluded that Chl-based calculations underestimate depth-integrated PP in the Arctic Ocean. These authors applied a relationship between the chl *a* concentration and PP at all depths and in the ZCHL_reg model. Thus, we can conclude that our results are consistent with those of Hill and Zimmerman. Additionally, our results are consistent with those of Carr et al. (2006). These authors noted that the simplest surface Chl-based model (Eppley et al., 1985) overestimated PP at high latitudes (in conditions of low PAR and T_0).

4.4. Advantages of the region-specific algorithms

Recent studies have reported the advantages of RSMs for AO IPP estimations (IOCCG, 2015; Y. Lee et al., 2015). Models that are developed with local databases operate with region-specific links between production characteristics and environmental factors. Theoretically, such models will perform better at local sites than algorithms that are created with datasets from other regions of the World Ocean.

We tested the predictive skill of some models that were developed for other Arctic Ocean regions (ArcPP) and the modified VGPM by using the Kara Sea dataset. The description of these models is given in the Supplementary material (S7). The results of the regression analysis and performance indices suggest that the VGPM with field P^b_{opt} data as an input variable demonstrated the best skill (Table 4; Fig. 7g) but overestimated the *in situ* IPP (B = 0.24). Recently, the VGPM exhibited the best results in the Arctic Ocean (Petrenko et al., 2013) and in the Southern California Current System (Jacox et al., 2015; Kahru et al., 2009).

The difficulties in P^b_{opt} application are the inability to use this parameter directly as the simplest input variable during both *in situ* and remote observations. When the VGPM is used for IPP estimations, $P^b{}_{opt}$ is calculated by using a polynomial equation that links $P^b{}_{opt}$ and T_0 (Behrenfeld and Falkowski, 1997a). No correlation between $P^b{}_{opt}$ and T_0 was observed during the autumn in the Kara Sea as shown in the Supplementary material (S8). Following Hill and Zimmerman (2010), we used the relationship between $P^b{}_{opt}$ and the incubation temperature to calculate IPP_{mod} (VGPM_Arc) (S7). These calculations demonstrated a significant decrease in the model skill ($R^2 = 0.60$; RMSD = 0.59; ME = − 0.60). Another approach is the application of the average trophic level $P^b{}_{opt}$ (Table 4) as an input variable (VGPM_TR). This method improved the model skill ($R^2 = 0.58$; RMSD = 0.37; ME = 0.37) compared to VGPM_Arc (Table 4). Finally, we verified the Chl-based ArcPP model (Hill et al., 2013) by using the Kara Sea dataset and vertical chl *a* distribution (Fig. 5). This algorithm was the least applicable to the Kara Sea ($R^2 = 0.47$; RMSD = 0.54; ME = − 0.34).

The average RMSD of the RSM and NRSM were equal to 0.34 ± 0.05 (*N* = 4) and 0.44 ± 0.13 (*N* = 4), respectively and their average model biases (modulo values) were 0.13 ± 0.09 (*N* = 4) and 0.35 ± 0.12 (*N* = 4), respectively. The region-specific models (except ZCHL_reg) underestimated or overestimated the *in situ* depth-integrated PP by a factor of 2. The NRSM overestimated the observed water column PP by a factor of 2.8. Thus, we can conclude that the region-specific algorithms performed better than the other models on average. However, we have to note that for all parameters the original VGPM showed highest or very similar skills than KSDRM and Ψ_MOD which were the best for the RSM and can get reasonable results in the Case II water body of the Kara Sea but, as mentioned above, using of VGPM in most cases is limited due to difficulties in determining of P^b_{opt}. The other NRSMs that were considered in the present article and that were developed based on Case I waters datasets (Gordon and Morel, 1983; Jerlov, 1968) are not appropriate to assess the Kara Sea's IPP.

Notably, the developed Kara Sea region-specific models that were assessed by field experiments performed no better than algorithms that were tested in previous works (Carr et al., 2006; Friedrichs et al., 2009; Saba et al., 2010, 2011). These models were developed based on data from different regions of the World Ocean, were validated at different sites, and over- or underestimated the water column PP by a factor of 2. Nevertheless, the developed RSM in the Kara Sea performed better than the NRSM and demonstrated advantages during application.

4.5. Influence of satellite-derived data input on the performance of the region-specific models

As mentioned above, the region-specific DIM (Ψ_MOD) and DRM (KSDRM) models performed equally when *in situ* data were used as input variables. Interestingly, the same conclusion could be reached when satellite-derived chl *a*, PAR and K_d were used for model validation (Table 5; Fig. 11). However, the application of satellite-derived data decreased the efficiency of both Ψ_MOD_{sat} and $KSDRM_{sat}$ in terms of the regression statistics, which is consistent with previous studies (Balch et al., 1992; Y. Lee et al., 2015).

Accurately determining the surface chlorophyll by remote sensing is critical to improve IPP estimation (*e.g.*, Y. Lee et al., 2015). As seen in Fig. 12a, the region-specific algorithm overestimated the *in situ* Chl_0 at values lower than 0.6 mg m^{-3}. Nevertheless, this algorithm is currently optimal because of the large errors of standard MODIS models in optically complex waters (IOCCG, 2015). Our findings suggest that MODIS OC3M overestimated Chl_{meas} by a factor of 3–5 in the Kara Sea, which is dominated by CDOM absorption. However, a good correlation was established between satellite-derived and measured PAR and K_d (Fig. 12b, c).

5. Conclusions

In this study, we presented the results of the development and skill assessment of region-specific Kara Sea depth-integrated and depth-resolved IPP algorithms. The performance of the developed models was compared to those of models that were used to evaluate Arctic Ocean depth-integrated primary production. For the first time, IPP algorithms were designed for Arctic Ocean Case II waters. We attempted to resolve this problem because we believe that the IPP in Case I and Case II waters must be assessed separately by using region-specific algorithms. The results of comparison of RSM's and NRSM's predictive skills suggest that the former are more effective in the Kara Sea than the latter.

The irradiance-dependent P^b_{opt} model and vertical chl *a* profiles in waters of variable productivity were applied for KSDRM parameterization. Generally, the results of the comparison between the DIM and DRM algorithms suggested that the depth resolution did not affect the model's performance.

Thus, our results implied that the model skill was increased through (1) a regional approach and (2) involving photophysiological phyto-

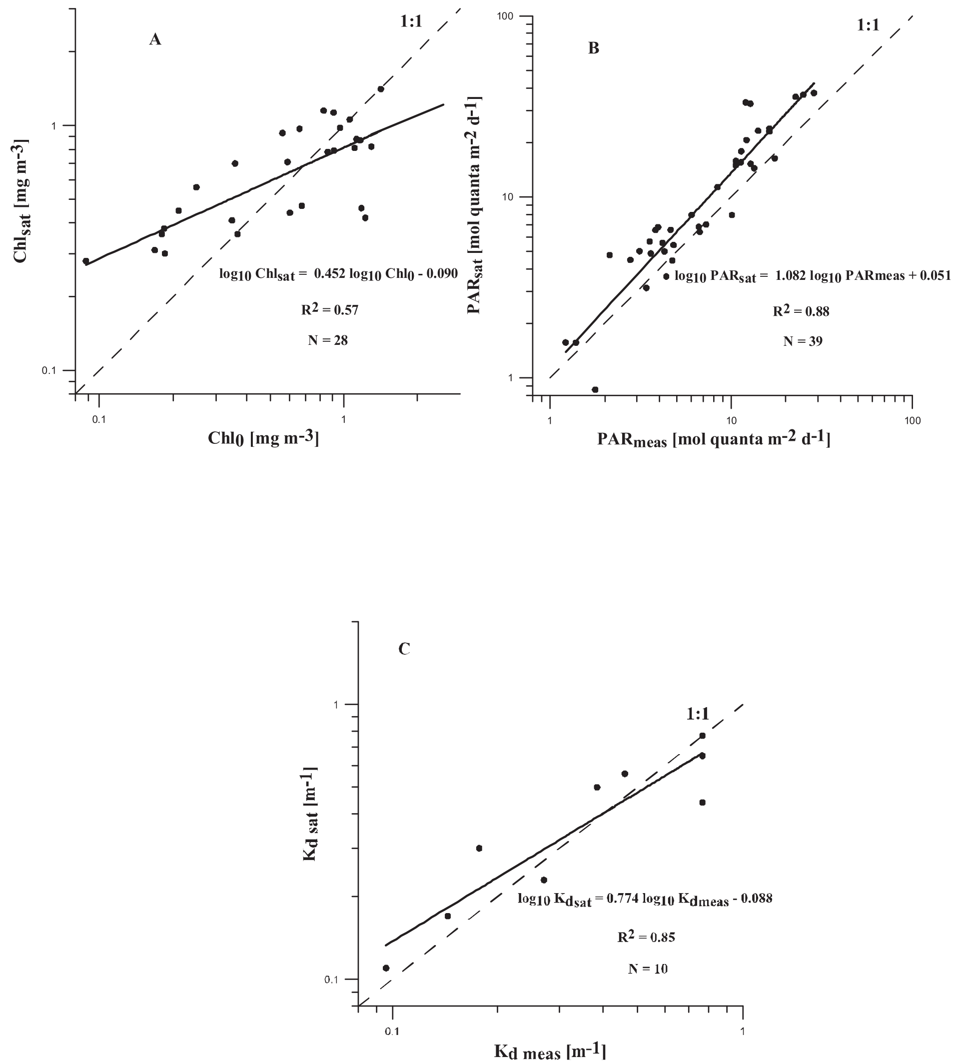

Fig. 12. Measured (*meas*) *vs.* satellite-derived (*sat*) values of surface chl *a* – (A); photosynthetically available radiation (PAR) – (B) and diffuse attenuation coefficient (K_d) – (C).

plankton characteristics such as the water column daily assimilation activity, efficiency of photosynthesis and incident solar radiation rather than using the chl *a* concentration as a single input variable. Thus, we consider the Ψ_MOD and KSDR algorithms to be the best for predicting Kara Sea IPP.

Model validation with satellite-derived parameters showed that region-specific DIM Ψ_MOD and DRM KSDRM performed equally. Apparently, Ψ_MOD had advantages compared to the KSDRM because of its simplicity. Therefore, we recommend using Ψ_MOD for Kara Sea IPP estimation.

In conclusion, we should mention the limitations of using the developed models. The examined algorithms were exclusively designed based on an autumn dataset and should be applied to IPP calculations in other seasons with some caution. Nevertheless, we consider that the region-specific depth-integrated algorithm (Ψ_MOD) currently can be implemented for IPP estimation in Arctic Ocean Case II waters by using satellite-derived datasets. Finally, increasing the *in situ* PP sample size and developing season-specific models is necessary to improve AO IPP evaluation.

Acknowledgments

We are grateful to the GSFC NASA for the MODIS data. Thanks are given to Simakova U.V. (P.P. Shirshov Institute of Oceanology, Russian Academy of Sciences) for assistance during the work at sea in 2011 and Stupnikova A.N. (P.P. Shirshov Institute of Oceanology, Russian Academy of Sciences) for the chlorophyll sample treatment during the work at sea in 2013 (125th cruise of R/V "Professor Shtokman"). We are also grateful to two anonymous reviewers for detailed reading, constructive criticism and useful recommendations. This work was supported by the Russian Foundation for Fundamental Research (project № 16-05-00050). Expeditionary observations and sample treatments were supported by the Russian Science Foundation (project № 14-50-00095, the scientific direction is "Ecosystems of strategically important marine regions of Russian Federation"). Development and application of satellite algorithms were supported by the Russian Science Foundation (project № 14-50-00095, the scientific direction is "Interaction of physical, biological and geological processes at coastal zone, shore waters and inland seas").

Appendix A. Supplementary material

Supplementary data to this article can be found online at http://dx.doi.org/10.1016/j.seares.2017.05.004.

References

Aitchison, J., Brown, J.A.C., 1957. The lognormal distribution. Econ. J. 67, 713–715.
Amon, R.M.W., 2004. The role of dissolved organic matter for the organic carbon cycle in the Arctic Ocean. In: Stein, R., Macdonald, R.W. (Eds.), The Organic Carbon Cycle in the Arctic Ocean. Springer-Verlag, Berlin, pp. 83–100.

Ardyna, M., Babin, M., Gosselin, M., Devred, E., Bélanger, S., Matsuoka, A., Tremblay, J.-É., 2013. Parameterization of vertical chlorophyll a in the Arctic Ocean: impact of the subsurface chlorophyll maximum on regional, seasonal and annual primary production estimates. Biogeosciences 10, 1345–1399.
Arrigo, K.R., van Dijken, G.L., 2011. Secular trends in Arctic Ocean net primary production. J. Geophys. Res. 116, C09011. http://dx.doi.org/10.1029/2011JC007151.
Arrigo, K.R., van Dijken, G.L., Bushinsky, S., 2008. Primary production in the Southern Ocean, 1997–2006. J. Geophys. Res. 113, C08004. http://dx.doi.org/10.1029/2007JC004551.
Arrigo, K.R., Matrai, P.A., van Dijken, G.L., 2011. Primary productivity in the Arctic Ocean: impact of complex optical properties and subsurface chlorophyll maxima on large-scale estimates. J. Geophys. Res. 116, C11022. http://dx.doi.org/10.1029/2011JC007273.
Babin, M., Bélanger, S., Ellingsen, I., Forest, A., Le Fouest, V., Lacour, T., Ardyna, M., Slagstad, D., 2015. Estimating of primary production in the Arctic Ocean using ocean color remote sensing and coupled physical-biological models: strengths, limitations and how they compare. Prog. Oceanogr. 139, 197–220.
Balch, W.M., Byrne, C.F., 1994. Factors affecting the estimate of primary production from space. J. Geophys. Res. 99, 7555–7570.
Balch, W.M., Evans, R., Brown, J., Feldman, G., McClain, C., Esaias, W., 1992. The remote sensing of ocean primary productivity: use of a new data compilation to test satellite algorithms. J. Geophys. Res. 97, 2279–2293.
Banse, K., Yong, M., 1990. Sources of variability in satellite-derived estimates of phytoplankton production in the Eastern Tropical Pacific. J. Geophys. Res. 95, 7201–7215.
Behrenfeld, M.J., Falkowski, P.G., 1997a. Photosynthetic rates derived from satellite-based chlorophyll concentrations. Limnol. Oceanogr. 42, 1–20.
Behrenfeld, M.J., Falkowski, P.G., 1997b. A consumer's guide to phytoplankton primary productivity models. Limnol. Oceanogr. 42, 1479–1491.
Behrenfeld, M.J., Marañon, E., Siegel, D.A., Hooker, S.B., 2002. A photoacclimation and nutrient based model of light-saturated photosynthesis for quantifying oceanic primary production. Mar. Ecol. Prog. Ser. 228, 103–117.
Bélanger, S., Babin, M., Tremblay, J.-E., 2013. Increasing cloudiness in Arctic damps the increase in phytoplankton primary production due to sea ice receding. Biogeosciences 10, 4087–4101.
Berger, W.H., 1989. Global maps of primary productivity. In: Berger, W.H., Smetacek, V.S., Wefer, G. (Eds.), Productivity of the Ocean: Present and Past. Wiley, Berlin, pp. 429–455.
Bidigare, R.R., Prezelin, B.B., Smith, R.C., 1992. Biooptical models and the problems of scaling. In: Falkowski, P.G., Woodhead, A.D. (Eds.), Primary Productivity and Biogeochemical Cycles in the Sea. Plenum Press, New York and London, pp. 175–212.
Brown, Z.W., Lowry, K.E., Palmer, M.A., van Dijken, G.L., Mills, M.M., Pickart, R.S., Arrigo, K.R., 2015. Characterizing the subsurface chlorophyll a maximum in the Chukchi Sea and Canada Basin. Deep-Sea Res. II 118, 88–104.
Brugel, S., Nozais, C., Poulin, M., Tremblay, J.-E., Miller, L.A., Simpson, K.G., Gratton, Y., Demers, S., 2009. Phytoplankton biomass and production in the southeastern Beaufort Sea in autumn 2002 and 2003. Mar. Ecol. Prog. Ser. 377, 63–77.
Burenkov, V.I., Golgin, Yu.A., Kravchishina, M.D., 2010. The distribution of the suspended matter concentration in the Kara Sea in September 2007 based on ship and satellite data. Oceanology 50, 798–805.
Campbell, J., Antoine, D., Armstrong, R., Arrigo, K., Balch, W., Barber, R., Behrenfeld, M., Bidigare, R., Bishop, J., Carr, M.-E., Esaias, W., Falkowski, P., Hoepffner, N., Iverson, R., Kiefer, D., Lohrenz, S., Marra, J., Morel, A., Ryan, J., Vedernikov, V., Waters, K., Yentsch, C., Yoder, J., 2002. Comparison of algorithms for estimating ocean primary production from surface chlorophyll, temperature, and irradiance. Glob. Biogeochem. Cycles 16. http://dx.doi.org/10.1029/2001GB001444.
Carder, K.L., Chen, F.R., Cannizzaro, J.P., Campbell, J.W., Mitchell, B.G., 2004. Performance of the MODIS semi-analytical ocean color algorithm for chlorophyll-a. Adv. Space Res. 33, 1152–1159.
Carr, M.-E., Friedrichs, M.A.M., Schmeltz, M., Aita, M.N., Antoine, D., Arrigo, K.R., Asanuma, I., Aumont, O., Barber, R., Behrenfeld, M., Bidigare, R., Buitenhuis, E., Campbell, J., Ciotti, A., Dierssen, H., Dowell, M., Dunne, J., Esaias, W., Gentili, B., Gregg, W., Groom, S., Hoepffner, N., Ishizaka, J., Kameda, T., Le Quéré, C., Lohrenz, S., Marra, J., Mélin, F., Moore, K., Morel, A., Reddy, T.E., Ryan, J., Scardi, M., Smyth, T., Turpie, K., Tilstone, G., Waters, K., Yamanaka, Y., 2006. A comparison of global estimates of marine primary production from ocean color. Deep-Sea Res. II 53, 741–770.
Cherkasheva, A., Nöthig, E.M., Bauerfeind, E., Melsheimer, C., Bracher, A., 2013. From the chlorophyll-a in the surface layer to its vertical profile: a Greenland Sea relationship for satellite applications. Ocean Sci. 9, 431–445.
Cota, G.F., Wang, J., Comiso, J., 2004. Transformation of global satellite chlorophyll retrievals with a regionally tuned algorithm. Remote Sens. Environ. 90, 373–377.
Demidov, A.B., Mosharov, S.A., 2015. Vertical distribution of primary production and chlorophyll a in the Kara Sea. Oceanology 55, 521–534.
Demidov, A.B., Mosharov, S.A., Gagarin, V.I., Romanova, N.D., 2011. Spatial variability of the primary production and chlorophyll a concentration in the Drake Passage in the Austral spring. Oceanology 51, 281–294.
Demidov, A.B., Mosharov, S.A., Makkaveev, P.N., 2014. Patterns of the Kara Sea primary production in autumn: biotic and abiotic forcing of subsurface layer. J. Mar. Syst. 132, 130–149.
Dittmar, T., Kattner, G., 2003. The biogeochemistry of the river and shelf ecosystem of the Arctic Ocean: a review. Mar. Chem. 83, 103–120.
Doney, S.C., Lima, I., Moore, J.K., Lindsay, K., Behrenfeld, M.J., Westberry, T.K., Mahowald, N., Glover, D.M., Takahashi, T., 2009. Skill metrics for confronting global upper ocean ecosystem-biogeochemistry models against field and remote sensing data. J. Mar. Syst. 76, 95–112.
Eppley, R., Steward, E., Abbott, E., Heyman, U., 1985. Estimating ocean primary production from satellite chlorophyll: introduction to regional differences and statistics for the Southern California Bight. J. Plankton Res. 7, 57–70.
Falkowski, P., 1981. Light-shade adaptation and assimilation numbers. J. Plankton Res. 3, 203–216.
Friedrichs, M.A.M., Carr, M.-E., Barber, R., Scardi, M., Antoine, D., Armstrong, R., Asanuma, I., Behrenfeld, M., Buitenhuis, E., Chai, F., Christian, J.R., Ciotti, A.M., Doney, S.C., Dowell, M., Dunne, J., Gentili, B., Gregg, W., Hoepffner, N., Ishizaka, J., Kameda, T., Lima, I., Marra, J., Mélin, F., Moore, K., Morel, A., O'Malley, R., O'Reilly, J., Saba, V., Schmeltz, M., Smyth, T., Tjiputra, J., Waters, K., 2009. Assessing the uncertainties of model estimates of primary productivity in the tropical Pacific Ocean. J. Mar. Syst. 76, 113–133.
Frouin, R., McPherson, J., Ueyoshi, K., Franz, B.A., 2012. A time series of photosynthetically available radiation at the ocean surface from SeaWiFS and MODIS data. Proc. SPIE 12. http://dx.doi.org/10.1117/1112.981264.
Gordon, H.R., 1989. Can the Lambert–Beer law be applied to the diffuse attenuation coefficient of ocean water? Limnol. Oceanogr. 34, 1389–1409.
Gordon, H.G., Morel, A., 1983. In: Barber, R.T., Mooers, N.K., Bowman, M.J., Zeitzschel, B. (Eds.), Remote Assessment of Ocean Color for Interpretation of Satellite Visible Imagery: A Review. Springer-Verlag, New York, pp. 114.
Hanzlick, D., Aagaard, K., 1980. Freshwater and Atlantic water in the Kara Sea. J. Geophys. Res. 85, 4937–4942.
Hegseth, E.N., 1997. Phytoplankton of the Barents Sea–the end of a growth season. Polar Biol. 17, 235–241.
Hill, V.J., Cota, G.F., 2005. Spatial patterns of primary production on the shelf, slope and basin of the Western Arctic in 2002. Deep-Sea Res. II 57, 3344–3354.
Hill, V.J., Zimmerman, R.C., 2010. Estimates of primary production by remote sensing in the Arctic Ocean: assessment of accuracy with passive and active sensors. Deep-Sea Res. I 57, 1243–1254.
Hill, V.J., Matrai, P.A., Olson, E., Suttles, S., Steele, M., Codispoti, L.A., Zimmerman, R.C., 2013. Synthesis of integrated primary production in the Arctic Ocean: II. In situ and remotely sensed estimates. Prog. Oceanogr. 110, 107–125.
Hirawake, T., Takao, S., Horimoto, N., Ishimaru, T., Yamaguchi, Y., Fukuchi, M., 2011. A phytoplankton absorption-based primary productivity model for remote sensing in the Southern Ocean. Polar Biol. 34, 291–302.
Holmes, R.M., McClelland, J.W., Peterson, B.J., Tank, S.E., Bulygina, E., Eglinton, T.I., Gordeev, V.V., Gurtovaya, T.Y., Raymond, P.A., Repeta, D.J., Staples, R., Striegl, R.G., Zhulidov, A.V., Zimov, S.A., 2012. Seasonal and annual fluxes of nutrients and organic matter from large rivers to the Arctic Ocean and surrounding seas. Estuar. Coasts 35, 369–382.
IOCCG, 2015. Ocean colour remote sensing in polar seas. In: Babin, M., Arrigo, K., Bélanger, S., Forget, M.-H. (Eds.), Reports of the International Ocean-Colour Coordinating Group. vol. 16 IOCCG, Dartmouth, Canada (130 pp.).
Isada, T., Hattori-Saito, A., Saito, H., Ikeda, T., Suzuki, K., 2010. Primary productivity and its bio-optical modeling in the Oyashio region, NW Pacific during the spring bloom 2007. Deep-Sea Res. II 57, 1653–1664.
Ishizaka, J., Siswanto, E., Itoh, T., Murakami, H., Yamaguchi, Y., Horimoto, N., Ishimaru, T., Hashimoto, S., Saino, T., 2007. Verification of vertically generalized production model and estimation of primary production in Sagami Bay, Japan. J. Oceanogr. 63, 517–524.
Jacox, M.G., Edwards, C.A., Kahru, M., Rudnik, D.L., Kudela, R.M., 2015. The potential for improving remote primary productivity estimates through subsurface chlorophyll and irradiance measurement. Deep-Sea Res. II 112, 107–116.
Jeffrey, S.W., Humphrey, G.F., 1975. New spectrophotometric equations for determining chlorophylls a, b, c_1 and c_2 in higher plants, algae and natural phytoplankton. Biochem. Physiol. Pflanz. 167, 191–194.
Jerlov, H.G., 1968. Optical Oceanography. Elsevier, New York, pp. 194.
JGOFS (Joint Global Ocean Flux Study Protocols), 1994. Protocols for the Joint Global Ocean Flux Study Protocols (JGOFS). In: Core Meas, Manual Guides, pp. 119–122.
Jolliff, J.K., Kindle, J.C., Shulman, I., Penta, B., Friedrichs, M.A.M., Helber, L., Arnone, R.A., 2009. Summary diagrams for coupled hydrodynamic-ecosystem model skill assessment. J. Mar. Syst. 76, 64–82.
Kahru, M., Kudela, R.M., Manzana-Sarabia, M., Mitchell, B.G., 2009. Trends in primary production in the California Current detected with satellite data. J. Geophys. Res. 114, C02004. http://dx.doi.org/10.1029/2008JC004979.
Koblentz-Mishke, O.I., Volkovinsky, V.V., Kabanova, Y.G., 1970. Plankton primary production of the world ocean. In: Wooster, W. (Ed.), Scientific Exploration of the South Pacific. National Academy of Sciences, Washington, D.C., pp. 183–193.
Kopelevich, O.V., Burenkov, V.I., Vazyulya, S.V., Sheberstov, S.V., Nabiullina, M.V., 2003. An assessment of the photosynthetically active radiation balance in the Barents Sea from the data of the SeaWiFS Satellite Ocean Color Scanner. Oceanology 43, 786–796.
Kubryakov, A., Stanichny, S., Zatsepin, A., 2016. River plume dynamics in the Kara Sea from altimetry-based lagrangian model, satellite salinity and chlorophyll data. Remote Sens. Environ. 176, 177–187.
Kuznetsova, O.A., Kopelevich, O.V., Sheberstov, S.V., Burenkov, V.I., Mosharov, S.A., Demidov, A.B., 2013. Estimation of chlorophyll concentration in the Kara Sea from data of MODIS-aqua satellite scanner. Issledovanie Zemli iz Kosmosa 5, 21–31 (in Russian).
Le Fouest, V., Babin, M., Ttemblay, J.-É., 2013. The fate of riverine nutrients on Arctic shelves. Biogeosciences 10, 3661–3677.
Lee, Y.J., Matrai, P.A., Friedrichs, M.A.M., Saba, V.S., Antoine, D., Ardyna, M., Asanuma, I., Babin, M., Bélanger, S., Benoît-Gagne, M., Devred, E., Fernández-Méndez, M., Gentili, B., Hirawake, T., Kang, Sung-Ho, Kameda, T., Katlein, C., Lee, S.H., Lee, Z., Mélin, F., Scardi, M., Smyth, T.J., Tang, S., Turpie, K.R., Waters, K.J., Westberry, T.K.,

2015a. An assessment of phytoplankton primary productivity in the Arctic Ocean from satellite ocean color/in situ chlorophyll-a based models. J. Geophys. Res. 120. http://dx.doi.org/10.1002/2015/JC11018.
Lee, Z., Marra, J., Perry, M.J., Kahru, M., 2015b. Estimating oceanic primary productivity from ocean color remote sensing: a strategic assessment. J. Mar. Syst. 149, 50–59.
Longhurst, A., Sathyendranath, S., Platt, T., Caverhill, C., 1995. An estimate of global primary production in the ocean from satellite radiometer data. J. Plankton Res. 17, 1245–1271.
Martin, J., Tremblay, J.-E., Gagnon, J., Tremblay, G., Lapoussiére, A., Jose, C., Poulin, M., Gosselin, M., Gratton, Y., Michel, C., 2010. Prevalence, structure and properties of subsurface chlorophyll maxima in Canadian Arctic waters. Mar. Ecol. Prog. Ser. 412, 69–84.
Martin, J., Tremblay, J.-E., Price, N.M., 2012. Nutritive and photosynthetic ecology of subsurface chlorophyll maxima in Canadian Arctic waters. Biogeosciences 9, 5353–5371.
Matrai, P.A., Olson, E., Suttles, S., Hill, V., Codispoti, L.A., Light, B., Steele, M., 2013. Synthesis of primary production in the Arctic Ocean: I. Surface waters, 1954–2007. Prog. Oceanogr. 110, 93–106.
McClain, C.R., Cleave, M.L., Feldman, G., Gregg, W., Hooker, S., Kuring, N., 1998. Science quality SeaWiFS data for global biosphere research. Sea Technol. 39, 10–16.
McClain, C.R., Feldman, G., Hooker, S.B., 2004. An overview of the SeaWiFS project and strategies for producing a climate research quality global ocean bio-optical time series. Deep-Sea Res. II 51, 5–42.
Megard, R.O., 1972. Phytoplankton, photosynthesis and phosphorus in Lake Minnetoka, Minnesota. Limnol. Oceanogr. 17, 68–87.
Morel, A., Berthon, J.-F., 1989. Surface pigments, algal biomass profiles, and potential production of the euphotic layer: relationships reinvestigated in view of remote-sensing applications. Limnol. Oceanogr. 34, 1545–1562.
Mosharov, S.A., 2010. Distribution of the primary production and chlorophyll a in the Kara Sea in September of 2007. Oceanology 50, 885–893.
Mosharov, S.A., Demidov, A.B., Simakova, U.V., 2016. Peculiarities of the primary production process in the Kara Sea at the end of the vegetation season. Oceanology 56, 84–94.
O'Reilly, J.E., Maritorena, S., Mitchell, B.G., Siegel, D.A., Carder, K.L., Garver, S.A., Kahru, M., McClain, C.R., 1998. Ocean color chlorophyll algorithms for SeaWiFS. J. Geophys. Res. 103, 24937–24953.
Pabi, S., van Dijken, G.L., Arrigo, K.R., 2008. Primary production in the Arctic Ocean, 1998–2006. J. Geophys. Res. 113, C08005. http://dx.doi.org/10.1029/2007/JC004578.
Petrenko, D., Pozdnyakov, D., Johannessen, J., Counillon, F., Sychov, V., 2013. Satellite-derived multi-year trend in primary production in the Arctic Ocean. Int. J. Remote Sens. 34, 3903–3937.
Pivovarov, S., Schlitzer, R., Novikhin, A., 2003. River run-off influence on the water mass formation in the Kara Sea. In: Stein, R., Fahl, K., Fütterer, D.K., Galimov, E.M., Stepanets, O.V. (Eds.), Siberian River Run-off in the Kara Sea. Elsevier, Amsterdam, pp. 9–25.
Platt, T., Sathyendranath, S., 1993. Estimators of primary production for interpretation of remotely-sensed data on ocean color. J. Geophys. Res. 98, 14561–14576.
Platt, T., Harrison, W.G., Horne, E.P.W., Irwin, B., 1987. Carbon fixation and oxygen evolution by phytoplankton in the Canadian High Arctic. Polar Biol. 8, 103–113.
Puigcorbé, V., Roca-Martí, M., Masqué, P., Benitez-Nelson, C.R., Rutgers, V.D., Loeff, M., Laglera, L.M., Bracher, A., Cheah, W., Strass, V.H., Hoppema, M., Santos-Echeandía, J., Hunt, B.P.V., Pakhomov, E.A., Klaas, C., 2017. Particulate organic carbon export across the Antarctic Circumpolar Current at 10° E: differences north and south of the Antarctic Polar Front. Deep-Sea Res. II. http://dx.doi.org/10.1016/j.dsr2.2016.05.016.
Rachold, V., Eicken, H., Gordeev, V.V., Grigoriev, M.N., Hubberten, H.-W., Lisitzin, A.P., Shevchenko, V.P., Schirrmeister, L., 2004. Modern terrigenous organic carbon input to the Arctic ocean. In: Stein, R., Macdonald, R.W. (Eds.), The Organic Carbon Cycle in the Arctic ocean. Springer-Verlag, Berlin, pp. 33–56.
Saba, V., Marjorie, S., Friedrichs, M.A.M., Carr, M.-E., Antoine, D., Armstrong, R.A., Asanuma, I., Aumont, O., Bates, N.R., Behrenfeld, M.J., Bennington, V., Bopp, L., Bruggeman, J., Buitenhuis, E.T., Church, M.J., Ciotti, A.M., Doney, S.C., Dowell, M., Dunne, J., Dutkiewicz, S., Gregg, W., Hoepffner, N., Hyde, K.J.W., Ishizaka, J., Kameda, T., Karl, D.M., Lima, I., Lomas, M.W., Marra, J., McKinley, G.A., Mélin, F., Moore, J.K., Morel, A., O'Reilly, J., Salihoglu, B., Scardi, M., Smyth, T.J., Tang, S., Tjiputra, J., Uitz, J., Vichi, M., Waters, K., Westberry, T.K., Yool, A., 2010. Challenges of modeling depth-integrated marine primary productivity over multiple decades: a case study at BATS and HOT. Glob. Biogeochem. Cycles 24, GB3020. http://dx.doi.org/10.1029/2009GB003655.
Saba, V.S., Friedrichs, M.A.M., Antoine, D., Armstrong, R.A., Asanuma, I., Behrenfeld, M.J., Ciotti, A.M., Dowell, M., Hoepffner, N., Hyde, K.J.W., Ishizaka, J., Kameda, T., Marra, J., Mélin, F., Morel, A., O'Reilly, J., Scardi, M., Smith Jr., W.O., Smyth, T.J., Tang, S., Uitz, J., Waters, K., Westberry, T.K., 2011. An evaluation of ocean color model estimates of marine primary productivity in coastal and pelagic regions across the globe. Biogeosciences 8, 489–503.
SCOR–UNESCO, 1966. Report of SCOR–UNESCO working group 17 on determination of photosynthetic pigments in Sea Water. In: Monography of Oceanography Methodology. vol. 1. UNESCO, Paris, pp. 9–18.
Sheberstov, S.V., Lukyanova, E.A., 2007. A system for acquisition, processing, and storage of satellite and field biooptical data. In: Proceedings of IV International Conference “Current Problems in Optics of Natural Waters”, Nizhny Novgorod, pp. 179–183.
Siegel, D.A., Westberry, T.K., O'Brien, M.C., Nelson, N.B., Michaels, A.F., Morrison, J.R., Scott, A., Caporelli, E.A., Sorensen, J.C., Maritorena, S., Garver, S.A., Brody, E.A., Ubante, J., Hammer, M.A., 2001. Bio-optical modeling of primary production on regional scales: the Bermuda BioOptics project. Deep-Sea Res. II 48, 1865–1896.
Smith, R.C., Baker, K.S., 1978. The bio-optical state of ocean waters and remote sensing. Limnol. Oceanogr. 23, 247–259.
Steemann Nielsen, E., 1952. The use of radioactive carbon (C^{14}) for measuring organic production in the sea. J. Cons. Int. Explor. Mer. 18, 117–140.
Stein, R., 2000. Circum Arctic river discharge and its geological record. Int. J. Earth Sci. 89, 447–449.
Stow, C.A., Jolliff, J., McGillicuddy Jr., D.J., Doney, C.S., Allen, J.I., Friedrichs, M.A.M., Rose, K.A., Wallhead, P., 2009. Skill assessment for coupled biological/physical models of marine systems. J. Mar. Syst. 76, 4–15.
Uitz, J., Claustre, H., Morel, A., Hooker, S.B., 2006. Vertical distribution of phytoplankton communities in open ocean: an assessment on surface chlorophyll. J. Geophys. Res. 111, C08005. http://dx.doi.org/10.1029/2005JC003207.
Vazyulya, S.V., Kopelevich, O.V., Sheberstov, S.V., Artemiev, V.A., 2014. Satellite estimation of the coefficients of CDOM absorption and diffuse attenuation in the White and Kara Seas. In: Current Problems of Earth Remote Sensing From Space. vol. 11. pp. 31–41 (in Russian).
Vazyulya, S.V., Kopelevich, O.V., Sheberstov, S.V., Artemiev, V.A., 2016. Estimation of sea surface solar radiation at 400–700 nm using satellite ocean color data. Opt. Express 24, A604–A611.
Vedernikov, V.I., Demidov, A.B., Sud'bin, A.I., 1994. Primary production and chlorophyll in the Kara Sea in September 1993. Oceanology 34, 630–640.
Vetrov, A.A., Romankevich, E.A., 2004. Carbon Cycle in the Russian Arctic Seas. Springer-Verlag, Berlin.
Vetrov, A.A., Romankevich, E.A., 2011. Primary production and fluxes of organic carbon to the seabed in the Russian arctic seas as a response to the recent warming. Oceanology 51, 255–266.
Vinogradov, M.E., Shushkina, E.A., Kopelevich, O.V., Sheberstov, S.V., 1996. Photosynthetic productivity of the world ocean from satellite and expeditionary data. Oceanology 36, 531–540.
Yun, M.S., Chung, K.H., Zimmerman, S., Zhao, J., Joo, H.M., Lee, S.H., 2012. Phytoplankton productivity and its response to higher light levels in the Canada Basin. Polar Biol. 35, 257–268.
Zatsepin, A.G., Zavialov, P.O., Kremenetskiy, V.V., Poyarkov, S.G., Soloviev, D.M., 2010. The upper desalinated layer in the Kara Sea. Oceanology 50, 658–668.
Zhai, L., Gudmundsson, K., Miller, P., Peng, W., Guðfinnsson, H., Debes, H., Hátún, H., White, G.N., Hernández Walls, R., Sathyendranath, S., Platt, T., 2012. Phytoplankton phenology and production around Iceland and Faroes. Cont. Shelf Res. 37, 15–25.